

## Late Pleistocene glacial advances, equilibrium-line altitude changes and paleoclimate in the Jakupica Mts (North Macedonia)

Zsófia Ruzsiczay-Rüdiger<sup>a,\*</sup>, Marjan Temovski<sup>a,b,\*</sup>, Zoltán Kern<sup>a</sup>, Balázs Madarász<sup>c</sup>, Ivica Milevski<sup>d</sup>, Johannes Lachner<sup>e</sup>, Peter Steier<sup>e</sup>

<sup>a</sup> Institute for Geological and Geochemical Research, Research Centre for Astronomy and Earth Sciences (MTA Centre of Excellence), ELKH Budaörsi út 45, 1112 Budapest, Hungary

<sup>b</sup> Isotope Climatology and Environmental Research Centre, Institute for Nuclear Research, Bem tér 18/c, 4026 Debrecen, Hungary

<sup>c</sup> Geographical Institute, Research Centre for Astronomy and Earth Sciences (MTA Centre of Excellence), ELKH, Budaörsi út 45, 1112 Budapest, Hungary

<sup>d</sup> Institute of Geography, Faculty of Natural Sciences and Mathematics, Ss. Cyril and Methodius University, Arhimedova 3, 1000 Skopje, Macedonia

<sup>e</sup> University of Vienna, Faculty of Physics - Isotope Physics, Austria

### ARTICLE INFO

#### Keywords:

Glacial geomorphology  
Cosmogenic nuclides  
Last glacial maximum  
Central Balkan Peninsula  
Equilibrium line altitude  
Glacio-climatological modelling

### ABSTRACT

In the Jakupica Mts a plateau glacier was reconstructed (max. area  $\sim 45 \text{ km}^2$ , max thickness:  $\sim 260 \text{ m}$ ). The study area comprises six formerly glaciated valleys, five of which were fed by the plateau glacier and one had an independent cirque when local glaciation reached its maximum ice extent (MIE). The equilibrium line altitude (ELA) of the most extended glacial phase was at  $2075^{+37}_{-25} \text{ m asl}$ . The  $^{10}\text{Be}$  cosmic ray exposure (CRE) age of this phase was estimated at  $19.3^{+1.7}_{-1.3} \text{ ka}$ , conformable with the Last Glacial Maximum (LGM). CRE ages from the next moraine generation placed the first phase of deglaciation to  $18.2^{+1.0}_{-3.0} \text{ ka}$ . The samples from the moraine of the penultimate deglaciation phase provided CRE ages with large scatter and biased towards old ages, which is probably the result of inherited cosmogenic nuclide concentrations within the rock.

Glacio-climatological modelling was performed for the MIE, which has a well-established LGM age. The degree-day model was used to calculate the amount of accumulation required to sustain the glaciological equilibrium assuming a certain temperature drop at the ELA. The degree-day model constrained by the pollen-based July paleo-temperature reconstructions yielded an annual total melt at the LGM ELA comparable to or slightly higher than the current mean annual precipitation at the same elevation. These wetter LGM conditions inferred from the paleo-glaciological evidence in Jakupica Mts suggest an enhanced moisture advection in the region.

### 1. Introduction

Geomorphological evidence of former glaciation was already reported across the currently mostly unglaciated Balkan Peninsula  $>100$  years ago (Cvijić, 1898, 1917, Oestreich 1902, Dedijer 1917). Since then an extensive work has started providing glacier reconstructions and a growing number of numerical ages constraining the timing of former glacier advances.

Extended Pleistocene glaciers and ice fields in the area were described in the coastal ranges along the Adriatic Sea, in such as the Velebit Mt. (Krklec et al., 2015; Sarikaya et al., 2020), Velež and Crvanj mountains (Žebre et al., 2019), Vran and Čvrsnica mountains, (Činer

et al., 2019) and the largest former ice cap covering  $\sim 65 \text{ km}^2$  area with  $\sim 450 \text{ m}$  ice thickness in the Orjen Mt. (Hughes et al., 2010). In the inland areas of the central Balkan Peninsula less extended Pleistocene glaciers and ice fields were reconstructed, e.g. in Central Montenegro (Hughes et al., 2011), Šar Mts (Kuhlemann et al., 2009), Rila Mts (Kuhlemann et al., 2013a), Pelister (Ribolini et al., 2018), Galičica Mt. (Gromig et al., 2018), Jablanica Mt. (Temovski et al., 2018; Ruzsiczay-Rüdiger et al., 2020) and Bistra Mt. (Isola et al., 2021) (Fig. 1A,B).

However, the results of the chronological work depict an ambiguous picture concerning the timing of the most extended glaciation and also on the glacier response to the cooling phases during the last deglaciation throughout the mountain ranges of the Balkan Peninsula and its

\* Corresponding authors at: Institute for Geological and Geochemical Research, Research Centre for Astronomy and Earth Sciences (MTA Centre of Excellence), ELKH Budaörsi út 45, 1112 Budapest, Hungary (M. Temovski).

E-mail addresses: [rrzsofi@geochem.hu](mailto:rrzsofi@geochem.hu) (Z. Ruzsiczay-Rüdiger), [temovski.marjan@atomki.hu](mailto:temovski.marjan@atomki.hu) (M. Temovski).

<https://doi.org/10.1016/j.catena.2022.106383>

Received 2 March 2022; Received in revised form 9 May 2022; Accepted 13 May 2022

Available online 1 June 2022

0341-8162/© 2022 The Authors. Published by Elsevier B.V. This is an open access article under the CC BY license (<http://creativecommons.org/licenses/by/4.0/>).

surroundings. Glacial chronologies established by U-series dating of secondary carbonates within moraines suggest that the most extensive glaciations occurred in the middle Pleistocene (Hughes et al., 2010, 2011), most probably during the Marine Isotope Stage 12 (MIS 12; 478–424 ka; Lisiecki and Raymo, 2005). Former existence of a major glaciation before the Last Glacial Maximum (LGM;  $22.1 \pm 4.3$  ka in the Northern Hemisphere; Shakun and Carlson, 2010) could not be identified by surface exposure dating of glacial landforms using in situ produced cosmogenic radionuclides (CRN)  $^{10}\text{Be}$  and  $^{36}\text{Cl}$ , so far. CRN ages of the landforms assigned to the largest glaciers pointed to the LGM in the central part of the peninsula (Kuhlemann et al., 2009, 2013a, Çiner et al., 2019; Ruzkiczay-Rüdiger et al., 2020), at certain coastal areas (Sarikaya et al., 2020) and at its northern margin (Kuhlemann et al., 2013b; Ruzkiczay-Rüdiger et al., 2016, 2021a).

As a further complication, indirect geochronological data assign a unique age to the local maximum ice extent in certain ranges such as MIS 8 (300–243 ka) in the Olympus Mt. (U-Th dating; Smith et al., 2006).  $^{36}\text{Cl}$  exposure durations of moraines placed the most extensive glaciation to the MIS 3 (57–29 ka) at Mt Chelmos (Pope et al., 2017) and to the Lateglacial (LG; the period between the LGM and the Holocene: ~18–11.6 ka) at Velež and Crvanj Mts (Žebre et al., 2019). Considering that the large number of new data acquired during the last decades provided apparently controversial geochronological information, recent

regional reviews (e.g., Leontaritis et al., 2020; Allard et al., 2021) stressed the need for further research in the wider Balkan region to establish the timing and extent of glaciations.

To meet this demand, our study focuses on the glacier reconstruction in the Jakupica Mts in North Macedonia, where glacial landscape is indicative of the former presence of several outlet glaciers descending from an extended ice cap to the surrounding valleys. The timing of the maximum ice extent (MIE) and subsequent glacier retreat is addressed by cosmic ray exposure (CRE) dating using in situ produced  $^{10}\text{Be}$ . The objectives of this research are i) to describe the glacial landforms and sediments of the study area; ii) to reconstruct the former glacier extent during the most extended glacial phase and subsequent deglaciation phases; iii) to provide an additional tie-point to the ambiguous question of the regional timing of the most extended glaciation; iv) use the reconstructed glaciers for the estimation of the equilibrium line altitude (ELA) of the area, and compare it to the regional record; and v) to make inferences about the climate conditions prevailing during the time of maximum ice extent.

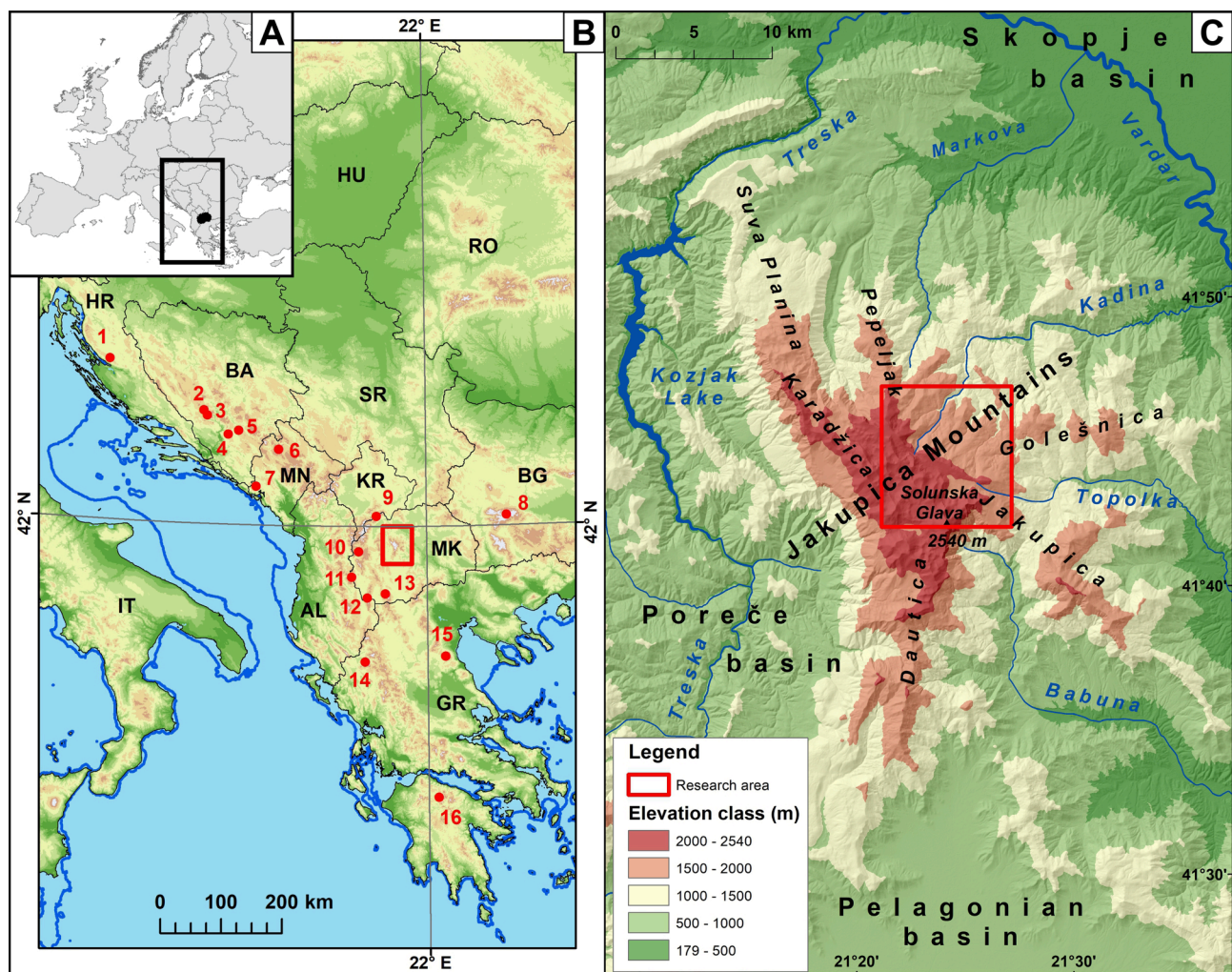


**Fig. 1.** The study area. A. location of Macedonia; B location of Jakupica Mts in the Balkan Peninsula. Mountain ranges mentioned in the text are shown by numbers: 1 – Velebit, 2 – Vran, 3 – Cvrstica, 4 – Velež, 5 – Crvanj, 6 – Durmitor, 7 – Orjen, 8 – Rila, 9 – Šar, 10 – Bistra, 11 – Jablanica, 12 – Galičica, 13 – Pelister, 14 – Pindus, 15 – Olympus, 16 – Chelmos. Thick blue line shows coastline at 120 m lower sea level (Zickel et al., 2016); C – Topography of the Jakupica Mts and location of the study area. The red rectangle frames Fig. 2a.

2. The study area

2.1. Geological and geomorphological setting

Jakupica Mts are a large mountain massif, located in North Macedonia (Fig. 1A-C), in the central part of the Balkan Peninsula. It is located along the eastern part of the Pelagonian Massif (Arsovski 1997), an Adria-derived unit within the Dinarides-Hellenides orogeny (Schmid et al. 2020). It is a horst structure, bounded to the south and west by the Pelagonian and Poreče Basins, respectively, facing with a well-expressed normal fault at the latter. To north and east it connects to the Skopje Basin and Vardar valley, respectively, with a more gradual morphological change (Fig. 1C). The basins surrounding the Jakupica Mts have formed from Middle Miocene to Pliocene times, as part of the South Balkan extensional system, the northern continuation of the Aegean

extensional regime (Dumurdžanov et al., 2004). Due to the lack of detailed studies on uplift rates of Macedonian mountains, it is very difficult to provide a reliable estimate for the Jakupica Mts during the Quaternary. Middle to Late Pleistocene valley incision rates in the southern parts of the Balkan Peninsula range from 0.23 to 0.96 mm/yr (Temovski et al., 2016; Pennos et al., 2019) with up to 1.8 mm/yr for tectonically more active areas (Smith et al., 1997; Palyvos et al., 2007). Based on the available regional data, and with the same approach used for Jablanica Mt. (Ruszkiczay-Rüdiger et al., 2020), an uplift rate of ~1 mm/yr was taken as a reasonable estimate for the Jakupica Mts.

Most of the mountain is built of metamorphic carbonate rocks that cover a crystalline basement composed of gneiss and micaschist with granitoid intrusions (Dumurdžanov et al., 1979, Jančevski et al., 1984, Arsovski 1997). The several hundred meters thick calcite and dolomite marble formation starts with a mica-rich marble (cipolin marble). The

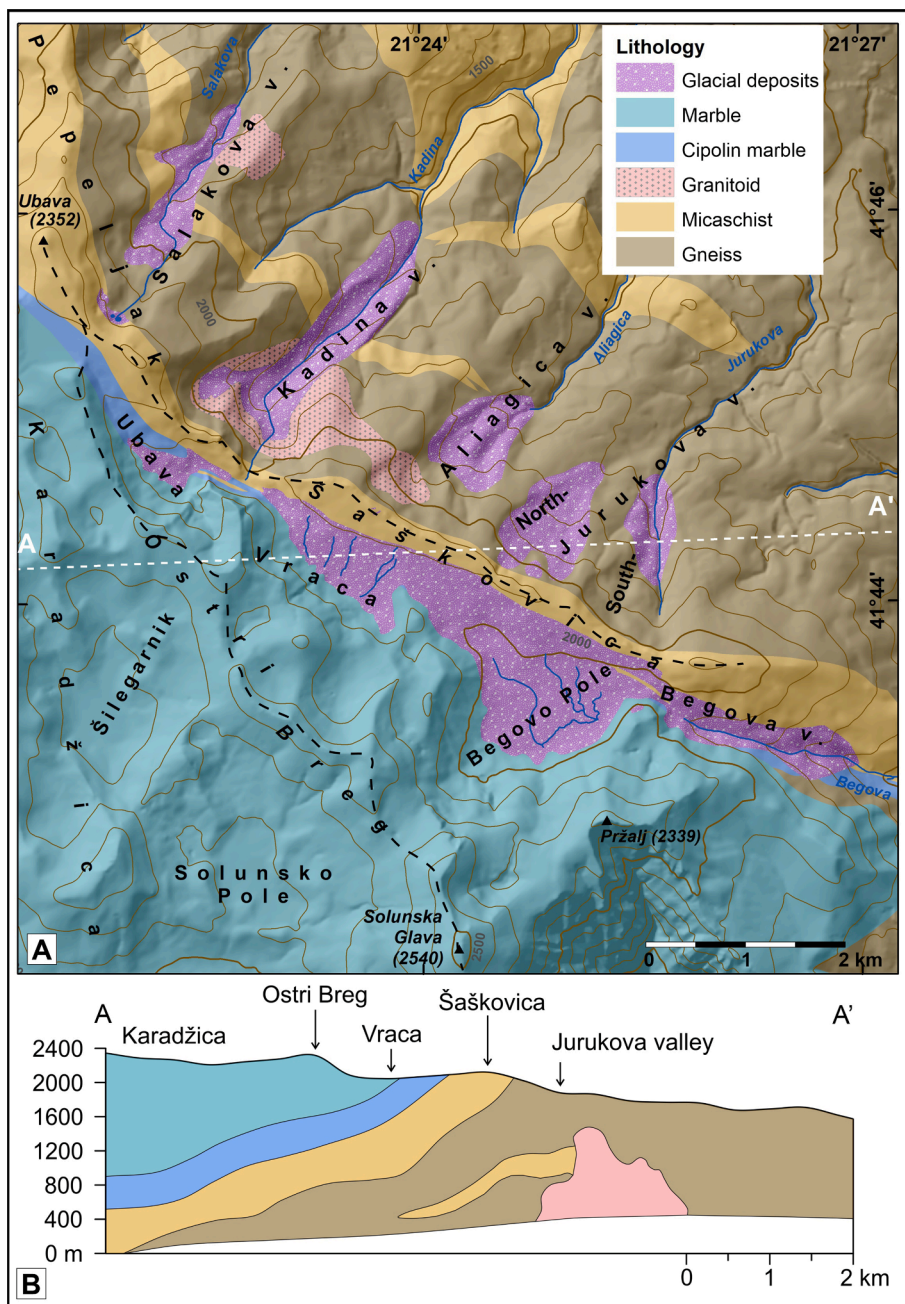


Fig. 2. A. Geological setting of the research area in the NE part of Jakupica Mts (modified from Jančevski et al., 1984). The Šaskovica and Ostri Breg ridges are indicated by dashed lines. B. The geological cross section of the study area (profile line A-A' on Fig. 1A).

south-western part of the mountain is developed entirely in the marble formation, whereas on the north-eastern part the basement rocks are exposed (Fig. 2). The crystalline rocks contain 20–47% quartz and are cut by numerous quartz veins (Jančevski et al. 1984).

The Jakupica Mts are characterised by a high central plateau, with the highest peak of Solunska Glava (2540 m), from which several mountain ridges extend radially (Fig. 1C), one of which (Jakupica Mt. sensu stricto) gave the name to the whole mountain massif (Jovanović 1928). The central plateau is segmented in a number of large, closed to semi-open depressions, sculptured by both karstic and glacial processes. It is a deeply karstified area, draining at several large karst springs located at elevations between 330 m and 1290 m (Temovski, 2018).

The main topographic drainage divide in the NE part of the plateau is the Ostri Breg ridge, a NNW-SSE oriented ridge starting at Ubava peak (2352 m) in the north and terminating at Solunska Glava (2540 m) in the south (Fig. 2A). This ridge divides the plateau into two parts: a smaller NE part with three large glacio-karstic depressions (Ubava, Vraca and Begovo Pole), and a larger, SW part also dissected by numerous glacio-karstic depressions (Fig. 2). The northeast border of the plateau is the Šaškovića ridge, a prominent NW-SE oriented ridge. It developed along the contact between the basement rocks and the overlying marble formation and rises gradually in elevation, from ~2000 m in the SE, up to 2352 m in the NW (Figs. 2, 3). This ridge represents the boundary between the dominantly glacio-karstic morphology found on the high central plateau to the southwest and several parallel NE-oriented, glacially overprinted valleys (from north to south: Salakova, Kadina, Aliagica, and Jurukova with two tributaries in its head, named here as Jurukova N and Jurukova S). Further to the SE another valley is descending from the plateau towards the east, called Begova valley (Fig. 2). Ostri Breg ridge was the main ice-divide of the former ice-field of the Jakupica Mts. The NE facing valleys of the study area were mostly fed by ice accumulated in the glacio-karstic depressions of Ubava, Vraca and Begovo Pole (Fig. 3).

The NE part of the Jakupica Mts plateau and the adjacent valleys are in the main focus of our study for three reasons: (i) It developed at the contact of different lithologies, allowing to recognise the possible contribution of the plateau ice to the valleys. (ii) The quartz-rich basement rocks in the valleys are suitable for  $^{10}\text{Be}$  exposure age dating, and thus to quantify the timing of the MIE and subsequent deglaciation phases in the area. (iii) The drainage divide towards the larger SW part of the former ice-field allows an independent glacier reconstruction in the NE area, which is necessary for the estimation of the paleo-ELAs of the mapped glacial phases.

## 2.2. The climate of the Jakupica Mts

The Jakupica Mts have typical mountain climate with cold winter, cool summer and no dry season (hemiboreal, Dfc according to the Köppen-Geiger classification; Peel et al., 2007). Based on the meteorological data in the period of 1951–1980, the mean annual air temperature (MAAT) at the Solunska Glava meteorological station (2540 m) is  $-0.6\text{ }^{\circ}\text{C}$ , the coldest month is February ( $-7.8\text{ }^{\circ}\text{C}$ ) and the warmest month is July ( $7.8\text{ }^{\circ}\text{C}$ ), with monthly mean temperatures  $<0\text{ }^{\circ}\text{C}$  from November to May (Lazarevski, 1993). The mean annual precipitation (MAP) based on the same period is 820 mm (Petreska, 2008). The highest monthly average precipitation is in May and December, and lowest in January and August. Snow cover remains until mid-June on flat areas, although it can stay until the end of August in dolines and depressions (Kolčakovski, 1988). Several caves in the plateau area are also known to host perennial ice and snow deposits (Temovski, 2018).

## 2.3. Previous research on glacial geomorphology of Jakupica Mts

Most of the previous research focused on the eastern parts of Jakupica Mts (Oestreich 1902, Gripp 1922, Milojević 1937, Manakovik 1966), with only Jovanović (1928) working on the whole massif. A brief overview of the main advances in the understanding of the glacial evolution is presented here, with an expanded version given in Supplement 1.3. The mentioned locations can be found on the map of Figs. 2 and 5.

Oestreich (1902) considered a single glacier that emerged NW from Ostri Breg ridge and was flowing in three directions: towards Salakova and Kadina valleys and to the SE through Ubava, Vraca and Begovo Pole depressions, possibly outflowing to Begova valley. Gripp (1922) also considered a single glacier, but flowing only to the SE through the depressions and finishing in Begovo Pole at ~2000 m. Jovanović (1928) interpreted glaciers descending down to elevations of ~1000 m. He also reconstructed a single glacier along the three depressions, flowing to the SE, but continuing further down to Begova valley, and reconstructed separate glaciers formed along the eastern side of the Šaškovića ridge. Jovanović (1928) identified five glacial stages, that, following the classical Alpine chronostratigraphic framework, he assigned to the Riss and Würm glacials and Bühl, Gschnitz and Daun stadials (Penk & Brückner, 1909), with the lowest ELA estimated at 1550 m and the highest at 2225 m asl. Milojević (1937) questioned the most extensive glacial stages proposed by Jovanović (1928), describing the lowest moraines at ~1700 m, and assigning the deposits at lower elevations as

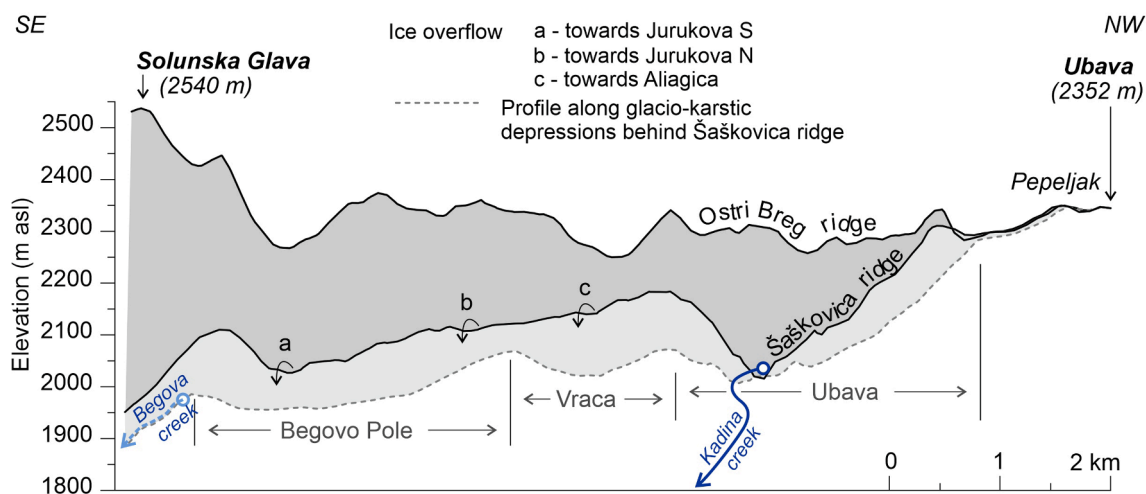


Fig. 3. Profiles of the ridges bounding the glacio-karstic depressions of the NE part of the Jakupica Mts plateau. Dashed line is the bottom of the Begovo Pole, Vraca and Ubava depressions. Curved arrows show the locations of past glacier overflow through the Šaškovića ridge from the depressions towards the NE valleys. a) and b) towards the Jurukova S and N valleys, c) towards the Aliagica valley. The location of the plotted ridgelines is indicated on Fig. 2.

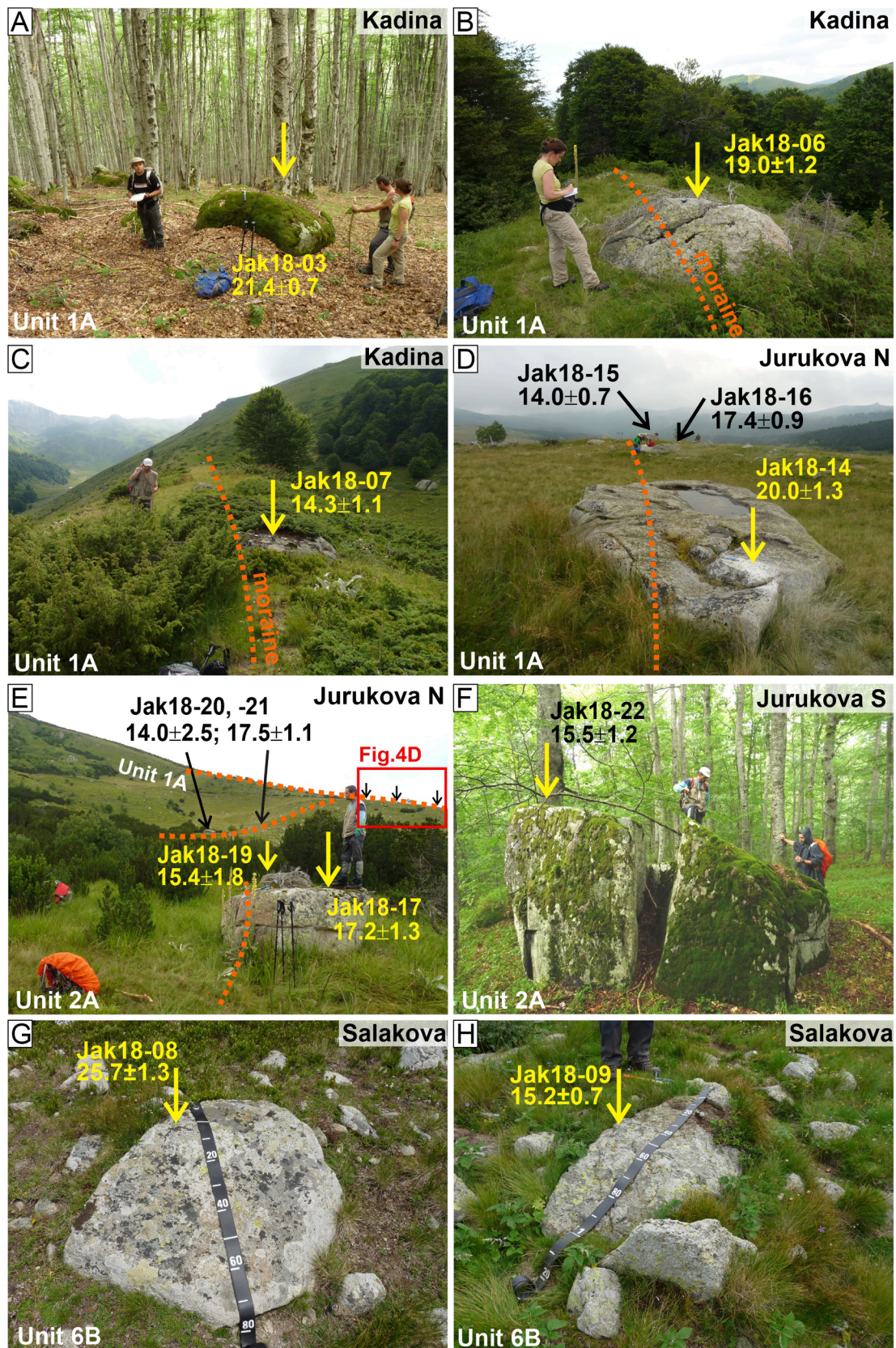
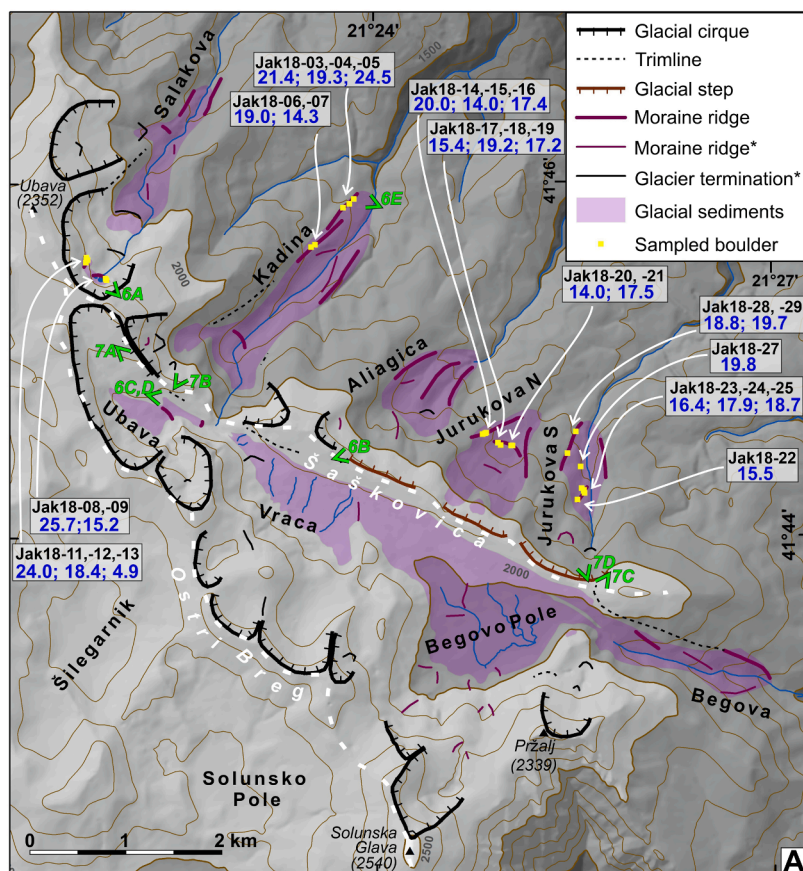
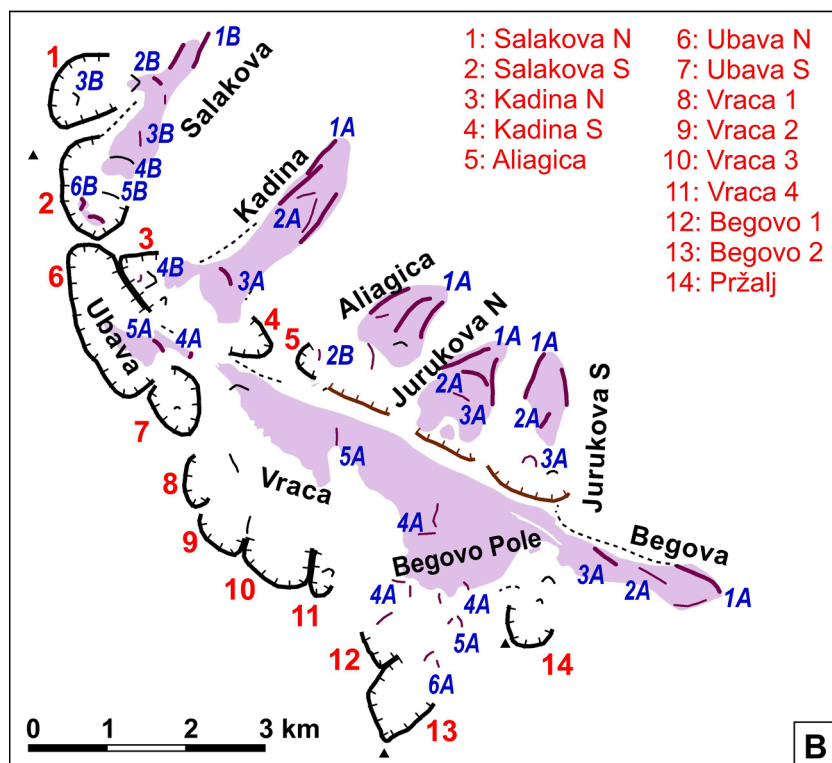


Fig. 4. Photos of some typical sample locations with their morphostartigraphic unit and CRE ages (ka). For locations of the sampled boulders refer to Fig. 5.



**Fig. 5. A:** Glacial geomorphology and glacial sediments of the Jakupica Mts. The prominent Ostri Breg and Šaskovica ridges are indicated by white dashed lines. In the legend \* indicates presumed landform. The CRE sample codes and ages (ka, no uncertainties indicated) appear in grey boxes, with black and blue colour, respectively. For data refer to Table 2. Green codes are locations of the photos in Figs. 6 and 7B: Line-drawing of the glacial cirques (black) and moraines (brown) of the study area. The blue codes refer to the position of the morphostratigraphic units (A indicates marble or mixed marble-crystalline boulder lithology; B indicates only crystalline boulder lithology), the red codes indicate the names used for the cirques throughout the text. Legend is the same as for Fig. 5A.



of either fluvial or fluvio-glacial origin. Milojević (1937) considered the glacier from Ubava depression to have continued into the Kadina valley and not towards the SE to Begovo Pole. He suggested that the glacier terminated on the plateau, in Begovo Pole towards the SE, and was not flowing out to Begova valley. Manakovik (1966) confirmed that the glacier from Begovo Pole was outflowing to the Begova valley, and supposed that during the stronger glaciations it must have been over-flowing also the Šaškovića ridge towards the NE.

### 3. Methodology

#### 3.1. Geomorphological mapping

Geomorphological mapping of glacial landforms (lateral and terminal moraines, cirques, glacially shaped valleys, trimlines, glacially polished surfaces) and distribution of glacial sediments were conducted on the basis of field investigations and combination of available data sources: topographic maps at 1:25 000 scale (Vojnogeografski Institut, 1973), a basic geological map in 1:100 000 scale (Dumurdžanov et al., 1979; Jančevski et al., 1984), GoogleEarth images at varying scales, and a 9 m resolution digital elevation model (DEM; Milevski et al., 2013). For cirque and cirque-floor delineation a combination of field identification, topographic maps, and DEM-derived contour and slope maps were utilized (Barr and Spagnolo, 2015). In the field a number of ground control points were collected using a hand-held GPS as a reference for the mapped geomorphological features. Digital cartographic work, morphometric analyses and final map production were done using Global Mapper (v17, Blue Marble Geographics, Hallowell, ME, USA) and ArcGIS (v10.1, ESRI, Redlands, CA, USA) softwares. The mapped moraines were classified into morphostratigraphic units based on their elevation, relative position, lithological characteristics and field observations on their preservation state (Hughes et al. 2005). The weakly expressed or poorly preserved features of the glacial morphology were identified as “presumed”. In case of the glacial termination, there is no identifiable moraine feature, but glacial termination is inferred either based on topographical expression (e.g., narrowing or bulging of valley floor), and/or increased density of scattered boulders. Both, presumed moraines or presumed glacial terminations were identified either directly on the field (e.g., in Kadina and Salakova valleys), or by a combination of fieldwork, satellite imagery, topographic map and DEM (e.g., in Aliagica, Begovo Pole and Vraca).

#### 3.2. Glacier reconstruction and ELA calculation

The shape and extent of the glaciers were reconstructed considering the mapped glacial landforms, like lateral and frontal moraines, trimlines and valley topography. The distribution of glacial sediments (Jančevski et al., 1984) was also used to constrain the maximum ice extent.

The glacier geometry of the ice field and outlet glaciers was reconstructed by the GlaRe, a semi-automated GIS-based method (Pellitero et al., 2016), using the 9 m DEM of the study area (Milevski et al., 2013). The ice thickness from the current bed topography was generated by the GlaRe toolbox applying the parametrisation used by Profiler v.2 (Benn and Hulton, 2010). The glacier thickness was adjusted to geomorphic markers by varying the basal shear stress value ( $\tau_b$ ). The most accepted values of the  $\tau_b$  vary within the ~50–150 kPa range with a possible increase to 190 kPa (Nye, 1952; Weertman, 1971; Vieira, 2008). In areas of low gradient and relatively shallow ice thickness  $\tau_b$  values of 20–80 kPa might be used (Žebre and Stepišnik, 2014). In this study, the maximum  $\tau_b$  values were monotonously decreased from 160 kPa used for the most extended phase to 30 kPa for the smallest glaciers to approximate the glacier thickness suggested by the geomorphic indices in each phase. On the low gradient plateaus, the applied  $\tau_b$  values were typically lowered, while at the glacial steps they were increased by 10–30 kPa with respect to the values used for the glacier tongues in a

certain phase.

In order to best reproduce the glacier surface, a combination of manual and semi-automated methods was used (Zasadni and Klapyta, 2014; Klapyta et al., 2021a, b). For the glacier tongues the glacier thickness along the flowline calculated by the GlaRe toolbox was extended manually to the valley sides taking into account the typical, slightly concave and convex shape of the glaciers above and below the ELA, respectively (Sissons, 1974). For the plateaus, the adjacent glacier surfaces were tuned to share a similar elevation and the ice-field was shaped to have a smooth, slightly updoming surface, typical of ice fields (Vieira, 2008; Cowton, et al., 2009; Žebre and Stepišnik, 2014).

The reconstructed glaciers and ice-field were used for the calculation of the former ELAs by means of the ELA Calculation toolbox (Pellitero et al., 2015) and applying the area-altitude balance ratio (AABR) method (Osmaston, 2005). The AABR method estimates the paleo-ELA considering the glacier hypsometry with a specific balance ratio representative of the climatic conditions of the study area. For the Jakupica Mts, the balance ratio of  $1.6 \pm 0.6$ , the median value recalculated from a global compilation (Rea, 2009; Zasadni et al., 2020), was adopted. This value was commonly used in paleoglaciological studies across the Carpathian and Balkan region (Ruzkiczay-Rüdiger et al., 2020; Zasadni et al., 2020; Klapyta et al., 2021a,b, 2022a), facilitating regional comparisons. It is very close to the recommended ratio of 1.56 by the recent global revision of AABR data (Oien et al., 2021). In the Dinaric area the  $1.9 \pm 0.81$  value, relevant for the mid-latitude maritime glaciers was also used (Žebre and Stepišnik, 2014; Žebre et al., 2019), which is still overlapping the uncertainty of the applied  $1.6 \pm 0.6$  balance ratio.

To estimate the characteristic ELA for the Jakupica Mts in each deglaciation phase, the ice-field and its outlet glaciers were treated as one unit, while valley glaciers with no connection to the ice-field were regarded as separate units with independent ELAs. During the MIE only the Salakova valley was considered to be independent from the ice-field, but throughout the subsequent deglaciation phases, the ice mass of the shrinking ice-field was split up into several glaciers. Therefore, the number of independent ELA estimates was growing parallel with the reduction of the glacier-covered area. The area-weighted mean of the individual ELA values was calculated as representative of each phase.

#### 3.3. Sampling strategy and sample collection for CRE age determination

The mapped terminal and lateral moraines were the major targets of sample collection. The boulders to be sampled were the largest possible and closest to the moraine crest. Their surface was to be flat with no signs of erosion or chipping (Balco, 2011, 2020) (Fig. 4). The samples were collected in 2018 using an angle grinder, hammer and chisel by chopping 1–3 cm thick chips from the rock surface. The position of the samples was measured using a hand-held GPS (Garmin etrex 30). The elevation of the samples was retrieved from the DEM. The strike and dip of the sampled surfaces were measured using a Suunto Tandem compass-clinometer. Altogether 27 samples for  $^{10}\text{Be}$  CRE dating were taken from three morphostratigraphic units of the study area. At least two, but preferably three or more samples were taken from each moraine to provide a solid basis for the age determination of the relevant deglaciation phase (Fig. 5A, B; Tables 1, S1).

Samples were taken from the moraines of the local MIE in three valleys. In the Kadina valley the MIE was represented by a double-crested lateral moraine from which five samples were collected. The terminal part of the moraine was destroyed by fluvial erosion. Samples Jak18-03 to -05 were collected from meter sized gneiss boulders near the moraine crest, close to the termination of the glacier tongue (Fig. 4. A). The position of the Jak18-05 sample was the closest to the moraine crest among the three samples. Two additional gneissic boulders were sampled (Jak18-06, -07) (Fig. 4. B,C) ~500 m further up-valley on the inner crest of the same moraine.

In the northern Jurukova (Jurukova N) valley three large gneissic boulders were sampled close to the junction of the lateral moraine of the

**Table 1**Sample data for cosmogenic  $^{10}\text{Be}$  exposure age determination. All sample and field data appear in Table S1.

Sample ID	Latitude (°)	Longitude (°)	Elevation (m, a.s.l.)	Thickness (cm)	Boulder size (cm)		
					length	width	height
Jak18-03	41.76514	21.39742	1589	1.0	240	230	130
Jak18-04	41.76470	21.39686	1598	0.8	340	270	160
Jak18-05	41.76431	21.39608	1609	1.6	200	195	120
Jak18-06	41.76086	21.39253	1678	1.1	210	160	80
Jak18-07	41.76063	21.39203	1689	1.5	180	120	55
Jak18-08	41.75774	21.36619	2177	2.0	110	95	20
Jak18-09	41.75759	21.36631	2178	1.5	120	75	40
Jak18-10	41.75951	21.36395	2194	2.0	130	65	30
Jak18-11	41.75973	21.36380	2193	1.3	70	80	30
Jak18-12	41.75926	21.36373	2200	0.8	70	40	30
Jak18-13	41.75926	21.36373	2200	3.0	70	50	30
Jak18-14	41.74295	21.41347	1820	1.5	600	350	170
Jak18-15	41.74309	21.41393	1814	2.0	260	165	120
Jak18-16	41.74302	21.41378	1816	2.0	310	300	80
Jak18-17	41.74187	21.41714	1772	1.0	230	210	120
Jak18-18	41.74186	21.41725	1772	2.5	390	300	260
Jak18-19	41.74189	21.41706	1772	1.0	175	200	75
Jak18-20	41.74191	21.41573	1780	2.8	450	410	130
Jak18-21	41.74214	21.41540	1783	2.0	170	110	80
Jak18-22	41.73675	21.42538	1746	1.0	420	330	280
Jak18-23	41.73766	21.42618	1727	1.0	260	130	80
Jak18-24	41.73736	21.42626	1729	1.2	140	140	70
Jak18-25	41.73756	21.42615	1728	1.8	260	190	80
Jak18-26	41.73783	21.42590	1728	2.1	430	330	260
Jak18-27	41.73985	21.42579	1701	1.6	900	700	320
Jak18-28	41.74114	21.42415	1725	1.5	240	160	100
Jak18-29	41.74316	21.42520	1689	1.3	280	160	110

MIE and terminal moraine of the subsequent phase (Jak18-14, –15, –16) (Fig. 4. D). Unfortunately, further away from the junction of the two landforms and closer to the terminal part of the moraine the lack of suitable boulders hampered sample collection. In the southern Jurukova (Jurukova S) valley, two samples were taken from gneiss boulders of the latero-frontal moraine complex of the MIE (Jak18-28, –29).

The moraine belonging to the second largest glacial phase could be sampled in the Jurukova-N and -S valleys. Five large gneiss boulders were sampled in the Jurukova N valley close to the crest of the frontal moraine (Jak18-17, –18, –19, –20 and –21) (Fig. 4.E). In the Jurukova

S valley one large boulder was sampled in a position between the moraines of the largest and second largest phase (Jak18-27). On the latero-frontal moraine of the second largest phase two large (Jak18-22, –26) (Fig. 4.F) and three moderate size boulders (Jak18-23, –24, –25) were sampled in beech forest. The boulders were covered by up to 2.5 cm thick moss cover.

Unfortunately, moraines of the subsequent three stages (Units 3, 4 and 5; Table 2 and Supplement 1.4) could not be sampled either due to the absence of suitable boulders or due to poor accessibility.

Three cirques in the northernmost part of the study area have

**Table 2**

Summary of the morphostratigraphy of glacial deposits as part of the NE Jakupica formation. Lit: boulder lithology; M: marble, C: crystalline rock.

Unit	Member	Location	Description	Lit.	Type locality	Lowest elevation
1	A:	Kadina, Aliagica, Jurukova N,	large lateral moraines.	M +	left lateral moraine below 1700 m in Kadina valley	~1550–1700 m
	Anište	Jurukova S, Begova		C		
2	B:	Salakova	lateral moraines	C	left lateral moraine in Salakova	~1670 m
	Salakova 1					
2	A:	Kadina, Aliagica, Jurukova N and S, Begova	lateral and terminal moraines.	M +	terminal moraine in Jurukova N., left lateral moraine in Jurukova S.	~1600–1770 m
	Jurukovi Bačila			C		
3	B:	Salakova, Aliagica	latero-terminal moraine, only	C	latero-terminal moraine in Salakova	~1830 m
	Salakova 2					
3	A:	Kadina, Begova, Jurukova N and S	lateral and terminal moraines	M +	left lateral in Begova, terminal in Kadina ~1750 m	~1750–1850 m
	Kadini Bačila			C		
4	B:	Salakova N and S	supposed lateral in Salakova	C	terminal moraine in Jurukova N.	~1800–1900 m
	Salakova 3					
4	A:	Ubava, Vraca, Begovo Pole, Przalj	small terminal moraines	M	small terminal moraine in Ubava near spring of Kadina Creek	~1970–2020 m
	Jurukova karpa			C		
5	B:	Salakova N and S, Aliagica.	supposed terminal moraines	C	terminal moraine in the Kadina N cirque	~1980–2020 m
	Salakova 4					
5	A:	Ubava, Vraca, Begovo Pole, Przalj	terminal moraines at Ubava and Vraca, supposed elsewhere	M	terminal moraine in Ubava at 2050 m.	~2050–2070 m
	Ubava			C		
6	B:	Salakova S	supposed glacier termination	C	no clear moraine, just prominent bulge in Salakova S	~2100 m
	Salakova 5					
6	A:	Ubava, Vraca, Begovo 2	supposed terminal moraines	M	terminal moraine in cirque below Solunska Glava	~2200 m
	Solunska			C		
Ezera	B:	Salakova S	terminal moraines in secondary cirques	C	terminal moraines in the in Salakova S cirque	~2190–2200 m
	Ezera					

developed in crystalline rocks: the Salakova N and S and the Kadina N cirques. In the Salakova S cirque the terminal moraines of the last deglaciation phase (Unit 6) were well developed, however the boulders were relatively small. Six samples were collected from small gneiss (Jak18-08, -09) (Fig. 4.G,H) and micaschist (Jak18-10) boulders and from boulders with quartz veins (Jak18-11, -12, -13) located on two terminal moraines assigned to this phase (Fig. 5A,B, 6A).

### 3.4. Determination of CRE ages

#### 3.4.1. Theory

Terrestrial in situ-produced cosmogenic  $^{10}\text{Be}$  is mainly produced from O and Si within quartz crystal lattice within the near-surface rocks. Surface exposure age of a rock is equal to the time it spent bombarded by cosmic rays (Lal, 1991; Gosse and Phillips, 2001). In most cases the  $^{10}\text{Be}$  CRE dating is well applicable in the  $10^3$  to  $10^5$  time range (up to  $10^2$ - $10^6$  years), thus it is suitable for the age determination of the landforms shaped by the Quaternary glaciations (Balco, 2011). Nevertheless, certain limitations are to be considered: the simple CRE age determination works on rocks that did not contain any CRN inventory at the moment of the creation of the landform to be dated. This so called inherited component, if present and remained unnoticed, would bias the CRE ages towards older apparent ages (Applegate et al., 2012; Briner et al., 2016; Çiner et al., 2017; Ruszkiczay-Rüdigier et al., 2021a). On the contrary, surface denudation and temporal shielding (e.g. by snow or soil) are reducing the CRN concentrations in the surface rocks, leading to younger apparent CRE ages. Accordingly, both processes are to be accounted for, when calculating and interpreting the apparent CRE ages (Heyman et al., 2011; Balco, 2011, 2020).

#### 3.4.2. Laboratory procedures

Sample processing was performed at the Cosmogenic Nuclide Sample Preparation Laboratory of the Institute for Geological and Geochemical Research (Budapest, Hungary)([https://www.geochem.hu/kozmogea n/Lab\\_en.html](https://www.geochem.hu/kozmogea n/Lab_en.html)) following the procedures of Brown et al., (1991) Merchel and Herpers, (1999) and Merchel et al. (2019) as described in Ruszkiczay-Rüdigier et al., 2021a,b). Purified BeO was mixed with Nb powder in 1:4 ratio and targets were prepared for AMS (Accelerator Mass Spectrometry) measurement of their  $^{10}\text{Be}/^9\text{Be}$  ratios at VERA, Vienna Environmental Research Accelerator, Faculty of Physics, University of Vienna (Steier et al., 2019). The beryllium measurements were normalized to the standard SMD-Be-12 (Akhmadaliev et al., 2013). This reference material is comparable with KNSTD (Nishiizumi et al., 2007) using a  $^{10}\text{Be}$  half-life of  $(1.387 \pm 0.012) \times 10^6$  years (Chmeleff et al., 2010; Korschinek et al., 2010). The uncertainty of the reference material (1.7%) is included in the reported uncertainties ( $1\sigma$ ).

#### 3.4.3. Calculation of exposure ages

Previous studies from the region demonstrated that CRE ages in the discussed time-range estimated using different time-dependent scaling methods (Lifton et al., 2014; Lifton, 2016) were statistically identical to those obtained via the Lal (1991)/Stone (2000) time independent scaling (Ruszkiczay-Rüdigier et al., 2020, 2021a). Therefore, in this study age calculations were performed using the time-independent Lal/Stone scaling using a sea level high latitude  $^{10}\text{Be}$  production rate of  $4.01 \pm 0.33$  at/gr/yr (Borchers et al., 2016) and the  $1.387 \pm 0.012$  Ma half-life of  $^{10}\text{Be}$  (Chmeleff et al., 2010; Korschinek et al., 2010), as described by Ruszkiczay-Rüdigier et al. (2020). The exposure ages were corrected for self-, slope- and topographic shielding, snow- and soil-shielding if relevant, for 1 mm/yr uplift rate (see section 2.1) and for 2 mm/ka surface denudation rate. The erosion rate was considered to be negligible for a single sample (Jak18-18) which was a quartz vein prepared from the bulk micaschist rock of the sampled boulder. The details of age determination, parameters and correction factors used throughout this study appear in Supplement 1.1. and Table S1.

In Table 4 CRE ages with only self and topographic shielding and

**Table 3**

Most important parameters of the reconstructed glaciers and the calculated ELAs using the AABR method (Osmaston, 2005) with a balance ratio of  $1.6 \pm 0.6$ . See detailed glacier reconstruction and ELA data in Table S3.

	Elevation of glacier termination (m asl)		Glacier area (km <sup>2</sup> )	Max. thickness (m)	ELA AABR 1.6 (m asl)	err+ (m asl)	err- (m asl)
	min	max					
Phase 6	2160	2243	1.43	77	2258	7	4
Phase 5	2037	2165	4.73	114	2196	13	8
Phase 4	1952	2103	7.07	163	2180	15	10
Phase 3	1763	1992	13.11	237	2171	18	13
Phase 2	1600	1837	15.96	256	2127	28	19
Phase 1	1493	1723	19.45	262	2075	35	27

with all corrections are reported (for more possibilities refer to Table S2). The applied correction factors are considered to be necessary to achieve the best estimate local production rate at each sample location. Therefore, in the following only the CRE ages with all corrections are discussed and used to derive the most probable exposure age of the glacial phases. The reported internal uncertainties of the CRE ages include the analytical uncertainties and the uncertainty of the half-life of  $^{10}\text{Be}$ . External uncertainties consider the uncertainty of the  $^{10}\text{Be}$  production rate as well (Table 2).

#### 3.4.4. Calculation of the most probable CRE age of the glacial stages

Calculation of the most probable exposure ages followed the methodology of Ruszkiczay-Rüdigier et al. (2020, 2021a). An important presumption was set by the relative chronological order of moraine generations, according to which the relative chronology of the moraine successions is a priori constrained by their morphostratigraphic position. In other words, each moraine left behind by a glacier still-stand of the deglaciation process is younger than its neighbour down-valley and is older than the subsequent moraine towards the valley head.

The individual CRE durations were grouped according to the mapped morphostratigraphic units. In case a morphostratigraphic unit was sampled in more than one valley, the obtained CRE ages were pooled together for the estimation of the most probable exposure age of the represented glacial phase. This approach is justified by the small horizontal distance and similar size and aspect of the studied valleys, which make diachronous glacier stabilization within the study area unlikely (Ruszkiczay-Rüdigier et al., 2020, 2021a).

For the estimation of the most probable CRE ages of a morphostratigraphic unit, samples with exposure durations overlapping within  $1\sigma$  uncertainties were considered. This method enables the identification of outliers until the examined group of data contains only CRE durations that are not significantly different considering associated  $1\sigma$  uncertainties (68% confidence interval). After the exclusion the statistical outliers, the most probable CRE age of the morphostratigraphic unit (i.e. a glacial phase) was estimated using cumulative probability density function (PDF) plots ("Camelplot" MATLAB code; Balco, 2009). The obtained  $^{10}\text{Be}$  CRE ages and their uncertainties at the 68% confidence interval ( $\pm 1\sigma$ ) are bracketing the most probable exposure age of moraine stabilization related to a certain glacial stage.

When ages of a single unit scatter more than what is expected from measurement uncertainty only, they reflect the effects of inheritance or post-depositional processes like denudation, toppling or temporal cover leading to old or young bias of the ages, respectively. In such cases the morphostratigraphic position of the landform may help to identify the process leading to the bias and the CRE age closest to the real landform

**Table 4**

Measured  $^{10}\text{Be}$  concentrations and calculated surface exposure durations. The measured AMS ratios were corrected for the average of four full processed blank ratios:  $(5.87 \pm 1.40) \times 10^{-15}$ . Age uncertainties: the 1st number is the “internal uncertainty” (analytical and half-life uncertainty;  $1\sigma$ ) and the 2nd number (in parenthesis) is the “external uncertainty”, which includes the uncertainty of the reference production rate. For all laboratory data and exposure ages calculated using different corrections refer to Table S2. \*Exposure age corrected for self-, slope- and topographic shielding. \*\* Exposure age corrected for self-, slope-, topographic-, snow- and soil shielding, 2 mm/kyr surface denudation and 1 mm/yr uplift. Outliers are printed in italics. The most probable exposure durations were calculated as described in section 3.4.4. and discussed in section 5.3.

Sample ID	Blank corrected $^{10}\text{Be}$ concentration (at/g <sub>SiO2</sub> )		Exposure duration (ka)		
			Basic correction*	All corrections**	Most probable
Unit 1					19.3 <sup>+1.7</sup> / <sub>-1.3</sub>
Jak18-03	277,242	±	8923	20.2 ± 0.7 (1.8)	21.4 ± 0.7 (1.9)
Jak18-04	255,909	±	13,378	18.3 ± 1 (1.8)	19.3 ± 1 (1.9)
<i>Jak18-05</i>	320,558	±	30,752	23 ± 2.2 (2.9)	24.5 ± 2.4 (3.1)
Jak18-06	263,287	±	16,243	18 ± 1.1 (1.9)	19.0 ± 1.2 (2)
<i>Jak18-07</i>	200,938	±	15,531	13.7 ± 1.1 (1.6)	14.3 ± 1.1 (1.6)
Jak18-14	308,678	±	19,909	19.1 ± 1.2 (2)	20.0 ± 1.3 (2.1)
<i>Jak18-15</i>	215,584	±	10,897	13.4 ± 0.7 (1.3)	14.0 ± 0.7 (1.4)
Jak18-16	265,779	±	13,827	16.5 ± 0.9 (1.6)	17.4 ± 0.9 (1.7)
Jak18-26	no current				
Jak18-27	271,554	±	14,355	18.8 ± 1 (1.8)	19.8 ± 1.1 (1.9)
Jak18-28	269,955	±	11,832	17.8 ± 0.8 (1.7)	18.8 ± 0.8 (1.8)
Jak18-29	276,267	±	14,381	18.7 ± 1 (1.8)	19.7 ± 1 (1.9)
Unit 2					18.2 <sup>+1.0</sup> / <sub>-3.0</sub>
Jak18-17	231,292	±	27,386	14.7 ± 1.7 (2.1)	15.4 ± 1.8 (2.2)
Jak18-18	291,631	±	11,449	18.8 ± 0.8 (1.7)	19.2 ± 0.8 (1.8)
Jak18-19	255,408	±	19,592	16.2 ± 1.3 (1.8)	17.2 ± 1.3 (1.9)
<i>Jak18-20</i>	208,273	±	37,438	13.4 ± 2.4 (2.6)	14.0 ± 2.5 (2.8)
Jak18-21	260,367	±	15,926	16.6 ± 1 (1.7)	17.5 ± 1.1 (1.8)
Jak18-22	223,595	±	17,722	14.8 ± 1.2 (1.7)	15.5 ± 1.2 (1.8)
Jak18-23	234,128	±	32,899	15.5 ± 2.2 (2.5)	16.4 ± 2.3 (2.7)
Jak18-24	253,375	±	15,682	16.9 ± 1.1 (1.7)	17.9 ± 1.1 (1.9)
Jak18-25	263,460	±	14,622	17.6 ± 1 (1.8)	18.7 ± 1 (1.9)
Unit 6					>15.2 ± 1.4
<i>Jak18-08</i>	483,138	±	23,625	23.8 ± 1.2 (2.3)	25.7 ± 1.3 (2.5)
Jak18-09	293,242	±	27,636	14.4 ± 1.4 (1.8)	15.2 ± 1.4 (1.9)
Jak18-10	no current				
<i>Jak18-11</i>	453,864	±	15,048	22.3 ± 0.8 (2)	24.0 ± 0.8 (2.1)
<i>Jak18-12</i>	354,805	±	11,253	17.3 ± 0.6 (1.5)	18.4 ± 0.6 (1.6)
<i>Jak18-13</i>	94,148	±	4759	4.7 ± 0.2 (0.5)	4.9 ± 0.2 (0.5)

age.

### 3.4.5. Glacio-climatological modelling

The degree-day model is used to calculate the amount of accumulation required to sustain a glaciological equilibrium (Brugger 2006, Hughes and Braithwaite 2008) assuming certain temperature drop at the ELA for the MIE glacial stage (Phase 1, Table 2).

Modern July mean temperature ( $T_{\text{July}}$ ) and MAP at the contours corresponding to the elevation of the paleo-ELA were retrieved from high-resolution gridded climate data (Milevski et al., 2015).  $T_{\text{July}}$  depression at the time of paleoglaciers was simulated from 4 °C and changed by 1 °C increments. In order to obtain the paleo- $T_{\text{July}}$ , a uniform temperature drop was assumed across the entire study area and was subtracted from the current gridded  $T_{\text{July}}$  (Milevski et al., 2015) corresponding to the ELA. The initial estimates of the course of daily mean temperature were distributed over a sine curve (Brugger 2006):

$$T_d = A \times \sin(2\pi \times d/\lambda - \Phi).$$

where  $T_d$  is the initial estimate of the mean daily air temperature,  $A$  is the half of the annual temperature range, which is the difference between the monthly mean temperature of the warmest and coldest months,  $d$  is the Julian day (1 to 365),  $\lambda$  is the period (365 days),  $\Phi$  is the phase angle (taken as 1.93 rad to reflect the fact that January is the coldest month).

First, the annual temperature range was set to 15.6 °C corresponding to the current monthly data of Solunska Glava (see section 2.2). Second, an increased annual temperature range was also considered reflecting the possibility that climate is likely to have been more continental during Pleistocene cold stages in this region (Hughes et al., 2011; Žebre et al., 2019). Since the regional estimates of the global pollen-based

paleo-temperature reconstruction at 21 ka (Cleator et al., 2020) show a 9 °C larger cooling for the coldest month compared to the warmest month in this region, the annual temperature range was set to 24.6 °C as an alternative scenario. The mean of the initial temperature estimates for July was subtracted from and paleo- $T_{\text{July}}$  was added to each Td to obtain a sinusoidal temperature variation throughout the year with the assumed paleo- $T_{\text{July}}$  and the chosen annual temperature range.

The amount of snow melt per day was calculated when  $T_d > 0$  °C using a degree-day factor of 4.1 mm day<sup>-1</sup>°C<sup>-1</sup> (Braithwaite, 2008). The annual accumulation required at the ELA to balance melting equals the sum of daily snow melt. The estimated annual accumulation total was expressed as the fraction of the current MAP at the corresponding ELA. It means that if its value is 1, the estimated accumulation is equal to the current MAP, while higher/lower fractions suggest wetter/drier paleo-climate conditions.

## 4. Results

### 4.1. Glacial morphology and stratigraphy

During fieldwork the NE part of the Jakupica Mts plateau and the studied valleys were visited, except for the higher cirques of the Ostri Breg ridge and the Aliagica valley, the latter of which was observed only from the Šaškovića ridge at its head. For these sites, the glacial features were mapped based on information from previous studies, DEM, topographic maps and satellite images.

Most of the glacial cirques of the study area have developed on the Ostri Breg ridge, which is the SW limit of our study area. These are semi-closed depressions, most of which have rather complicated morphology,

due to their polygenetic, glacio-karstic origin. Few of them though, have simpler, glacial-cirque-like morphology, with steeper headwalls and much lower open side (e.g., the cirque below Solunska Glava; Fig. 5A). Glacial cirques, generally poorly developed, can be found also in the

crystalline rocks, along the higher northeastern parts of Šaškovica ridge, in the head of the Salakova and Kadina valleys. The cirques are oriented mostly in NE to E direction, except those in the Kadina and Ubava valleys having SE and NW aspect (Fig. 5A,B).

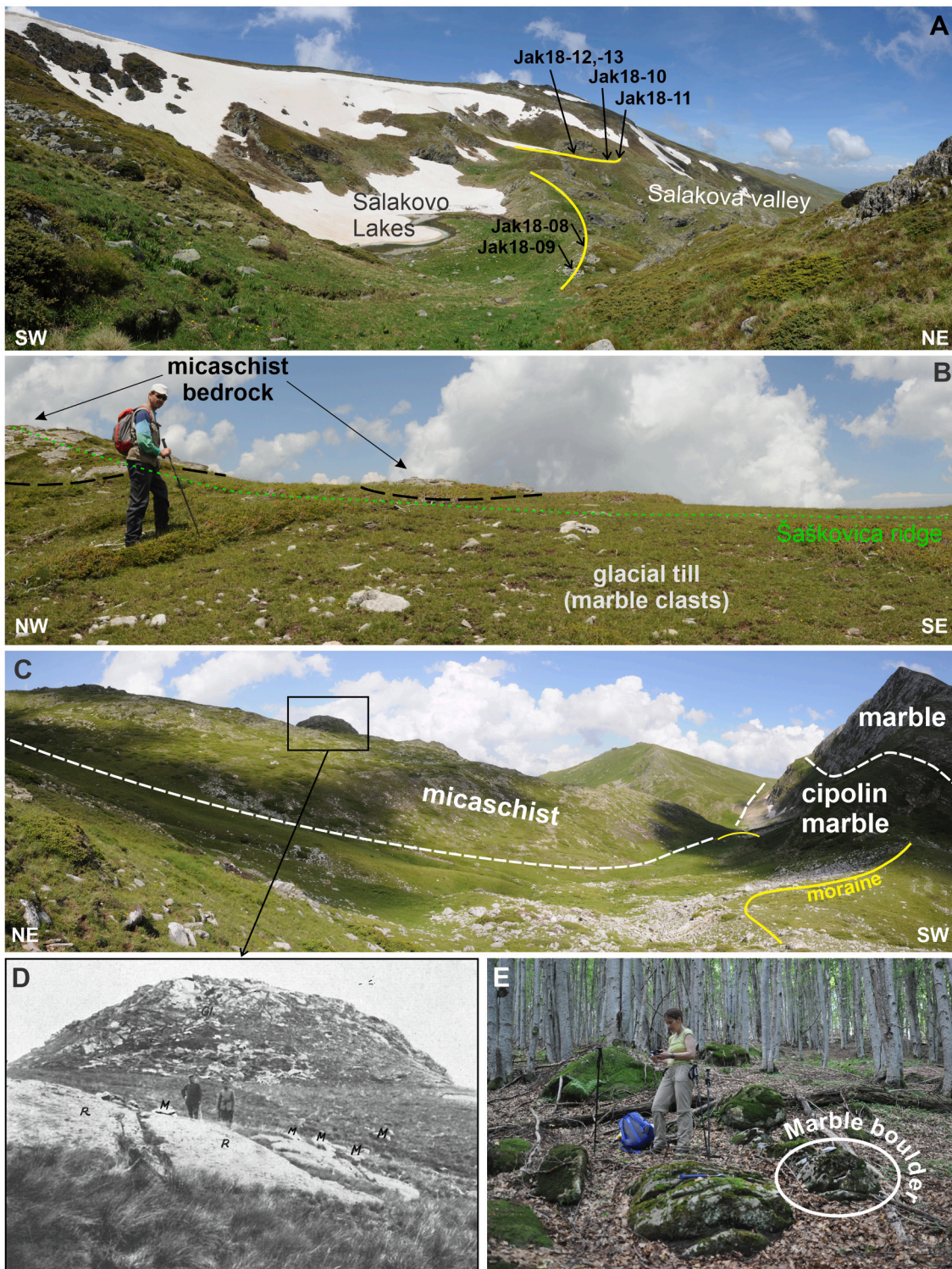


**Fig. 6.** Glacial landscape and occurrences of marble boulders on crystalline lithology proving that the plateau glacier was overflowing the Šaškovica ridge. (A) The cirque of the Salakova valley, with moraines of the Unit 6B and sample locations for CRE dating. (B) Glacial till with marble clasts covering the Šaškovica ridge above the Aliagica valley. (C) Panoramic view of the Ubava depression with the Units 5A and 4A moraines and Šaškovica ridge with the location of marble clasts already described by Gripp (1922). White dashed lines are the lithological boundaries. (D) the photo from Gripp (1922), where “R” indicates roche moutonnée, and “M” shows the location of marble clasts. The location of the photo can be identified by the rounded peak in the background. (E) Marble boulder among the crystalline ones in the Unit 1A moraine of the Kadina valley. For locations refer to Fig. 5A.

Glacial deposits on the plateau are mostly glacial till composed only of marble boulders in various sizes (mostly up to 1 m in diameter), covering the lower parts of the three large depressions. Glacial till is found also covering the micashist bedrock on the inner, plateau-side of the Šaškovica Ridge, with marble boulders found as erratics on top of micashist bedrock at few locations along Šaškovica Ridge (e.g., at the

Ubava depression, as reported also by Gripp (1922)). These erratics along with the marble boulders found in the moraines of Units 1–3 (Table 2) indicate that the plateau ice was flowing over the Šaškovica Ridge into the Kadina, Aliagica and Jurukova valleys (Fig. 6B,C,D, 7A; C).

The studied valleys have wide, U-shaped morphology, with Kadina

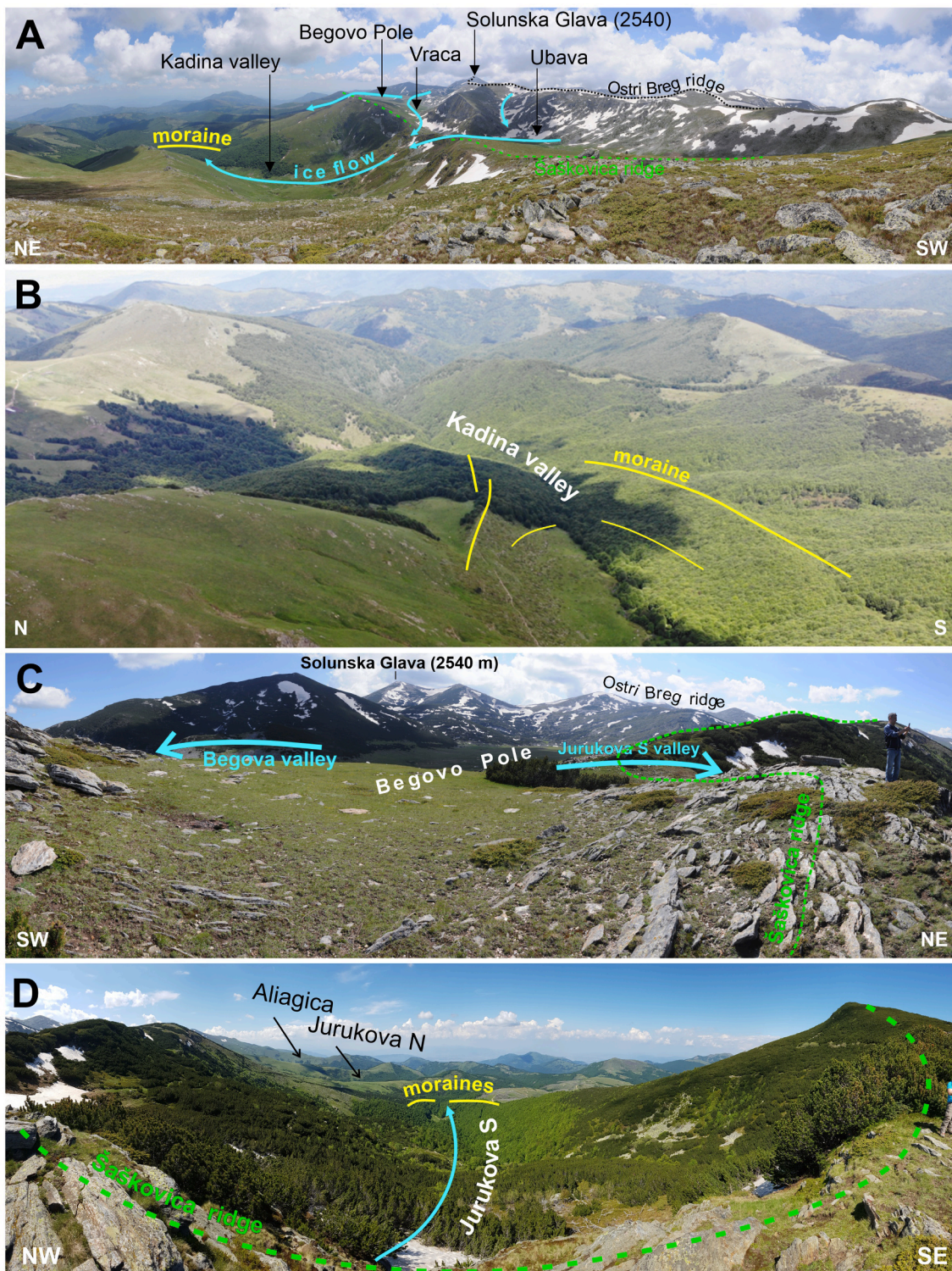


**Fig. 7.** Glacial landscape of the NE Jakupica Mts (A) Panoramic view of the NE part of the Jakupica Mts plateau with the Ostri Breg ridge, the former ice divide, the Šaškovica ridge and the directions of glacial outflow from the plateau to the NE facing valleys. (B) View of the Unit 1A and 2A moraines in the Kadina valley. (C) Panoramic view of the northern part Jakupica Mts plateau from the southeastern end of the Šaškovica ridge with the outflow directions of the former icefield. (D) Panoramic view of the Jurukova S valley from the Šaškovica ridge with the moraines of the maximum ice extent (Unit 1A). For locations refer to Fig. 5A.

valley having the deepest and longest glacial trough (Figs. 5, 7B,D). Glacial till composed of boulders of mixed marble and crystalline lithology is found down to elevations of 1500–1700 m in Kadina, Aliagica and Jurukova valleys. In Salakova valley, glacial till is composed only of crystalline boulders and found down to elevations of ~1670 m.

The Begova valley, descending to the SE from Begovo Pole along the contact of the crystalline and marble formations, also has the morphology of a glacial trough. In the upper parts it receives a short tributary valley that emerges from a poorly developed cirque below Pržalj peak (2339 m) (Fig. 5A,B). This is the lowest elevation outlet of the former ice-field. Glacial sediments composed of marble and mica-chist boulders are found down to an elevation of ~1550 m.

The glacial deposits mapped in the NE part of Jakupica Mts were classified within the same glacial formation: the Northeast Jakupica Formation. This formation contains 6 units corresponding to their morphostratigraphic position. Each unit has two members distinguished by lithological criteria: (A) containing or completely composed of marble boulders, reflecting ice contribution from the high karst plateau; (B) composed only of crystalline rocks, indicating no or insignificant contribution of ice from the high karst plateau (Fig. 5A,B). Summary of the morphostratigraphic units is given in Table 2, and detailed description in Supplement 1.4.

#### 4.2. Glacier reconstruction and ELA calculation

During the MIE an extensive ice-field covered the entire plateau of the Jakupica Mts. It had several outlet glaciers occupying the valleys descending from the plateau in all directions (Fig. 8). The area of the whole ice-field was ~46 km<sup>2</sup> with a maximum thickness of ~260 m (Figs. 8, 9A). The glaciers descended to ~1500–1700 m asl. (Table 3).

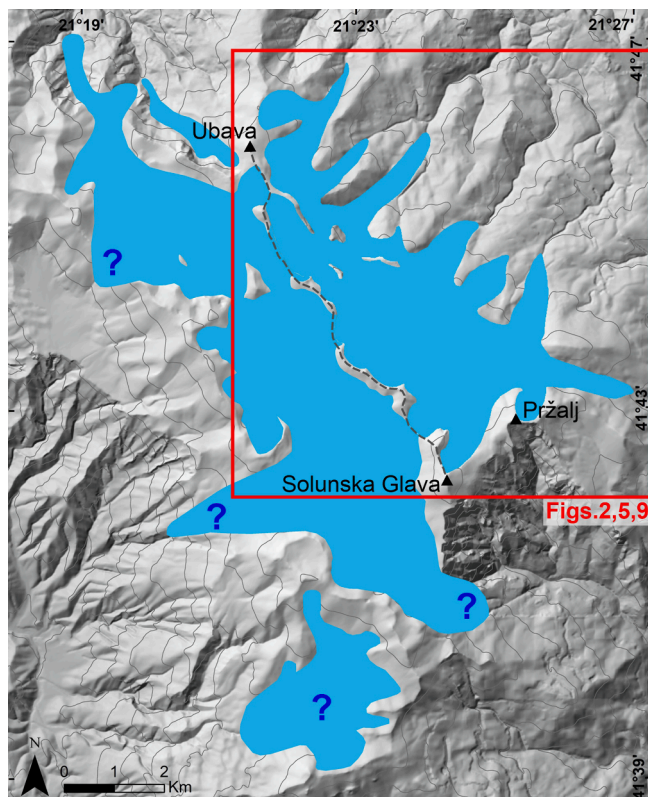


**Fig. 8.** The reconstructed maximum ice extent of the ice-field covering the Jakupica Mts. The question marks show locations where the ice margins are uncertain. The black dashed line is the current topographic divide, the Ostri Breg ridge, which supposedly was the ice divide between the northeastern and southwestern parts of the Jakupica ice-field. The red frame shows the location of Fig. 2, 5, 9.

The geochronological work was done on the glacier tongues descending from the smaller, north-eastern area of the former ice-field, which was separated from the south-western area by the Ostri Breg ridge. Therefore, this area was subject of the detailed glacier reconstructions and ELA calculations for each mapped glacier phase (Fig. 9, Table 3 and S3).

During the MIE the area of the north-eastern part of the Jakupica ice-field was ~19.5 km<sup>2</sup> (Fig. 9A). The Jurukova and Aliagica valleys were fed by the ice descending from the plateau flowing over the Šaškovica ridge, reaching elevations of ~1650–1720 m asl. At the Kadina valley the ridge was cut through and the glacier was fed directly from the cirque area at Ubava. This glacier reached down to ~1490 m, the lowest glacier termination of the study area. The glacier tongue descending eastward from the Begovo Pole in the Begova valley had the lowest outlet point. It had a lower gradient compared to the Kadina valley thus reached down to the second lowest elevation of ~1560 m asl. The Šaškovica Ridge is the highest on the NW, where it served as an ice divide between the northern part of the ice-field and the Salakova valley. As a consequence, this valley had an independent cirque with no ice input from the ice-field. The mean ELA during this phase is estimated at 2075<sup>+35</sup>/<sub>-27</sub> m.

During the second and third largest phases the glacier tongues fed by the ice-field were shortening, reaching elevations of ~1600–1840 m and ~1760–1990 m asl, respectively (Fig. 9B,C). The glaciated area shrank first to ~16.0 km<sup>2</sup> then to ~13.1 km<sup>2</sup> with only a slight decrease of the maximum ice thickness to ~256 then to ~237 m. The reconstructed ELA for these phases is 2127<sup>+28</sup>/<sub>-19</sub> m and 2171<sup>+18</sup>/<sub>-13</sub> m, respectively.

By the fourth phase of deglaciation the former ice-field was fragmented into several smaller glacier tongues descending from the peak region of the Ostri Breg ridge onto the plateau (Fig. 9D). Accordingly, the Kadina, Aliagica, Jurukova and Begova valleys were deglaciated by this phase. The cirques of the Salakova valley, being independent from the ice-field and reaching elevations comparable to the cirques of the Ostri Breg ridge hosted small glaciers. The ELA of this phase is reconstructed at 2180<sup>+15</sup>/<sub>-10</sub> m asl. As the deglaciation reached the low gradient plateau area between the third and fourth phases, the relatively small change in the ELA led to a considerable shrinkage in the glacier area to ~7.1 km<sup>2</sup> and glacier thickness to ~163 m.

During the last two deglaciation phases the glaciers were further shrinking, occupying a total area of ~4.7 km<sup>2</sup> and 1.4 km<sup>2</sup> with a maximum thickness of ~115 m and ~75 m in the fifth and sixth phases, respectively (Fig. 9E,F). The ELA was at 2196<sup>+13</sup>/<sub>-8</sub> m in the penultimate and at 2258<sup>+7</sup>/<sub>-4</sub> m during the last phase.

#### 4.3. The <sup>10</sup>Be concentrations and calculated CRE ages

The measured <sup>10</sup>Be/<sup>9</sup>Be ratios were between  $(1.16 \pm 0.05) \times 10^{-13}$  and  $(5.75 \pm 0.26) \times 10^{-13}$ . The mean <sup>10</sup>Be/<sup>9</sup>Be ratio of four processed blanks was  $(5.87 \pm 1.40) \times 10^{-15}$  resulting in a mean blank correction of 2.54%. Two out of 27 samples gave no current during the AMS measurements. The measured <sup>10</sup>Be concentrations ranged from  $(94.1 \pm 4.8) \times 10^3$  at/g<sub>SiO2</sub> to  $(483.1 \pm 23.6) \times 10^3$  at/g<sub>SiO2</sub>. The mean analytical uncertainty was 6.8% (Table 4).

The exposure durations corrected for self-, slope-, topographic-, snow- and soil shielding, for 2 mm/ka surface denudation and 1 mm/yr uplift rate are considered to be the best estimate of the age of deglaciation. Therefore, these are discussed in the text but ages with no correction are reported in Table 4, as well. In Table S2 further versions of ages with limited corrections appear.

The calculated exposure durations of the moraines representing the maximum ice extent (Unit1) were between  $24.5 \pm 2.4$  ka and  $14.0 \pm 0.7$  ka. The oldest (Jak18-05) and the two youngest ages (Jak18-07 and -15) failed to overlap within 1 $\sigma$  uncertainty with the rest of the group. Therefore, these were considered as outliers (Fig. 11A). The CRE durations of the remaining eight samples were between  $21.4 \pm 0.7$  ka and

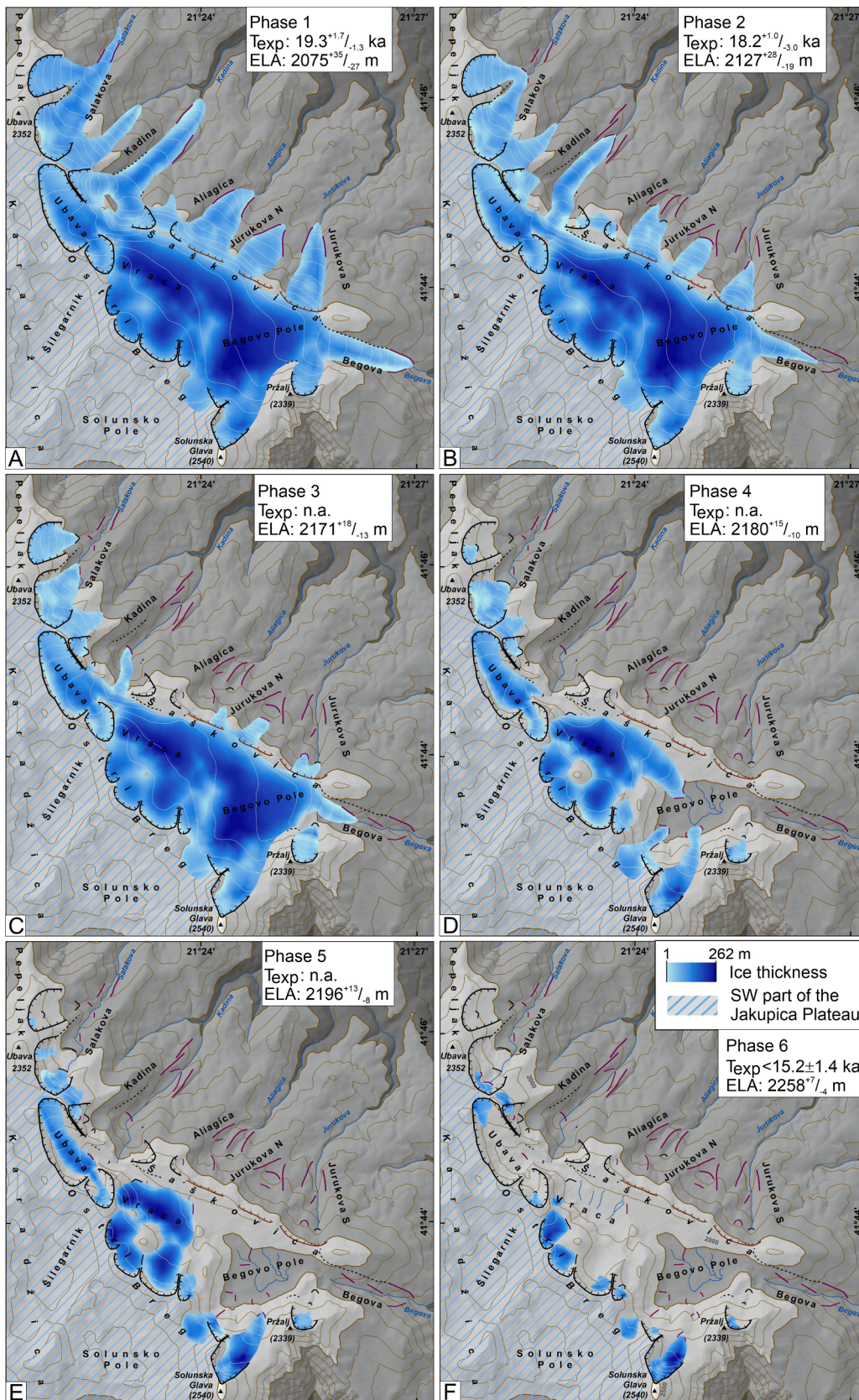
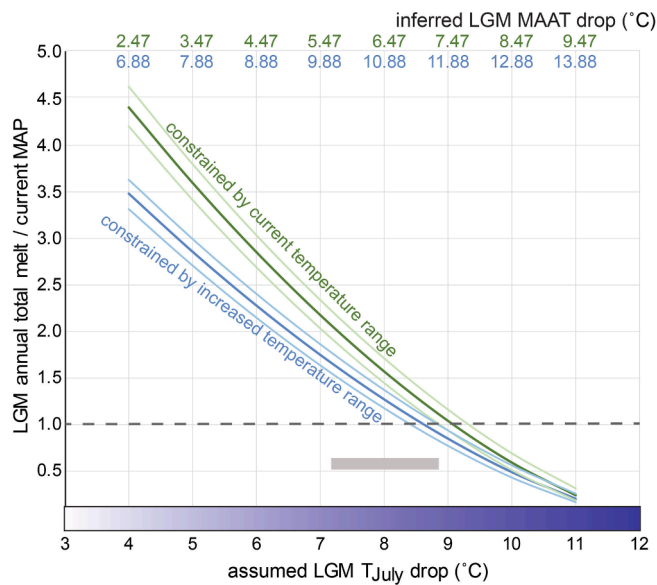


Fig. 9. Results of glacier reconstruction on the NE part of the Jakupica Mts. The legend is as on Fig. 5A, the contour line interval is 100 m.



**Fig. 10.** Paleoclimate conditions necessary to sustain LGM glaciers in the Jakupica Mts considering 4 to 11 °C drop in July mean temperature ( $T_{\text{July}}$  drop °C) and both current and increased annual temperature ranges. The curves represent the fraction of simulated annual total melt during the LGM to the current MAP (1951–1980 period; Milevski et al., 2015) assuming current (green) and increased (blue) annual temperature ranges. The lighter curves bracketing the mean represent  $\pm 1\text{SD}$  uncertainty calculated from the estimates of each valley. For data refer to Table S4. Estimates of the corresponding drops of MAAT are indicated at the top of the plot (with the same colour code). The grey rectangle indicates the pollen-based estimates (Cleator et al., 2020) of  $T_{\text{July}}$  cooling and fraction of LGM MAP to current MAP in the area of Jakupica Mts.

$17.4 \pm 1.3$  ka. These samples form a coherent group, and thus were used to determine the most probable age of moraine stabilization (Table 4, Fig. 5).

The CRE age of the sampled boulders of the second largest phase (Unit2) ranged from  $19.2 \pm 0.8$  ka and  $14.0 \pm 2.5$  ka. The youngest sample (Jak18-20) of this sample group was considered as an outlier due to its exceptionally high uncertainty (18%) (Fig. 11B). The remaining eight samples between  $19.2 \pm 0.8$  ka and  $15.4 \pm 1.8$  ka form a coherent age group and were used for the calculation of the most probable CRE age of the second largest deglaciation phase (Table 4, Fig. 5).

The samples from the last phase of deglaciation (Unit 6) yielded CRE durations with a wide scatter between  $25.7 \pm 1.3$  ka and  $4.8 \pm 0.2$  ka (Fig. 11C). The lack of coherence between the sample ages and the age distribution covering  $>20$  kyrs suggest that the sampled boulders might have been affected by inheritance and/or post-depositional disturbances (Balco, 2011; Heyman et al., 2011) (Table 4, Fig. 5). Due to the large scatter in this sample group no statistical method could be used for the exclusion of outliers.

#### 4.4. Glacio-climatological modelling for the LGM

The results of degree-day model calculations for the individual paleoglaciers appear in Table S4. The averaged values appear on Fig. 10. One of the interesting outcomes of the glacio-climatological modelling is the  $\sim 4.4\text{C}$  larger drop of the estimated LGM MAAT assuming the same drop in  $T_{\text{July}}$  using an increased temperature range compared to the model using the current temperature range. Another striking feature is the larger modelled precipitation required to maintain the glaciological equilibrium considering the current annual temperature range compared to the scenario assuming an increased seasonality (Fig. 10, Table S4). This is in agreement with the general expectations about the effect of increased seasonality on glacier mass balance (Golledge et al., 2010), but strangely contrasts to other glacio-climatological modelling

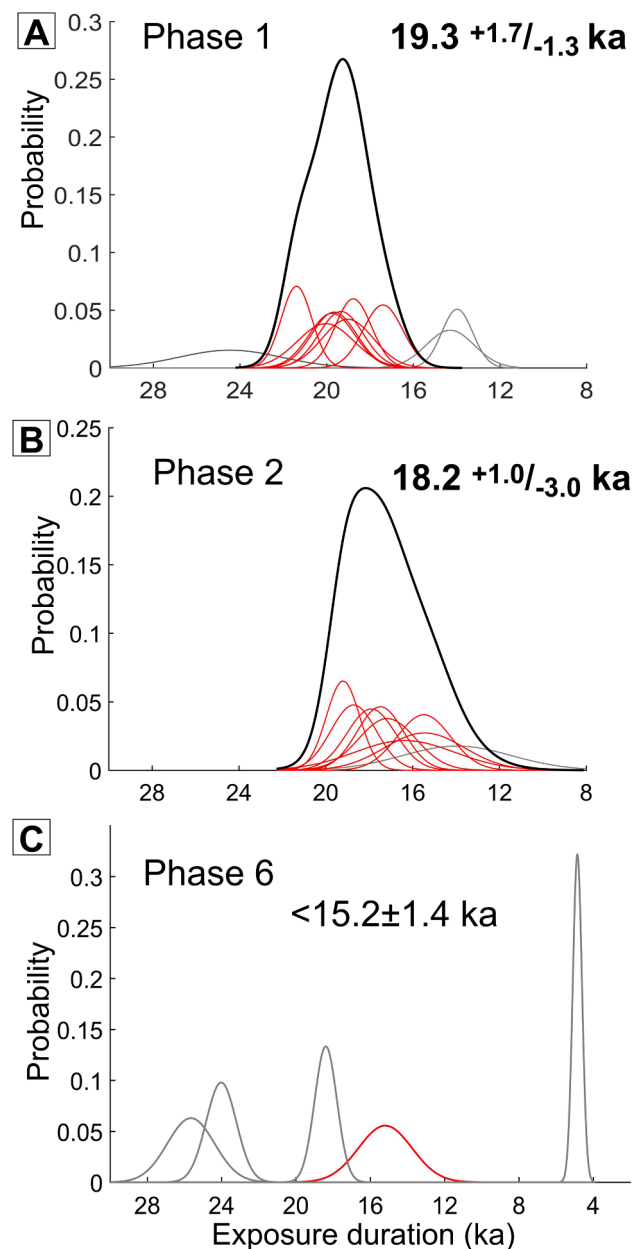


**Fig. 11.** Probability density function plots of the dated glacial phases. Red and grey curves are the accepted and rejected CRE ages of the individual samples, respectively. The black lines are the probability density functions (PDF) of the accepted samples. It was not possible to fit a PDF to the samples of the Unit 6 due to the large scatter of the resultant CRE ages. A: The MIE (Unit1); B: the 2nd largest phase (Unit 2); C: The last glacial phase (Unit 6).

results (Hughes et al., 2011; Žebre et al., 2019); however, this might stem from methodological differences.

The degree-day modelling yielded zero accumulation at the paleo-ELA for certain glacier basins running the model with a  $T_{\text{July}}$  drop  $>11\text{C}$ . As zero accumulation and zero ablation at the ELA are not realistic, no scenarios below  $11\text{C}$   $T_{\text{July}}$  drop were considered (Table S4; Fig. 10). Hence, the paleo-glaciological evidence argues that in the Jakupica Mts the maximum conceivable cooling of the warmest month during the LGM was  $\sim 11\text{C}$ . This is in agreement with independent regional data on LGM climate, derived from the most recent paleoecological evidence (Cleator et al., 2020; Sümeği and Gulyás, 2021) and noble gas-based paleotemperature estimates of groundwater in the surroundings that recharged  $\sim 20$  thousand years ago (Varsányi et al., 2011; Seltzer et al., 2021).

## 5. Discussion

### 5.1. Most probable CRE age of the dated landforms/glacial phases

After the exclusion of the statistical outliers, the PDF of the coherent group of eight samples belonging to the MIE (Unit 1) provided a most probable age of  $19.3^{+1.7}/_{-1.3}$  (Fig. 9A; 10A). This exposure age suggests that the moraine stabilization occurred in the later part of the LGM. The CRE age of the oldest sample, excluded from the determination of the most probable age, may indicate that the LGM glacier expansion reached its maximum length already at  $24.5 \pm 2.4$  ka, and remained stable at this position for several millennia.

After the exclusion of an outlier, the most probable CRE age of Unit 2 determined by the PDF of the remaining eight samples was  $18.2^{+1.0}/_{-3.0}$  ka, placing the onset of the deglaciation of the Jakupica Mts to the beginning of the Lateglacial (Fig. 9B; 10B).

Unfortunately, the CRE ages of the samples from moraines of Unit 6 show a large scatter. The youngest sample (Jak18-13) provided a mid-Holocene age, much younger than the age of complete deglaciation in the mountain ranges of similar elevation in the region (e.g., Kuhlemann et al., 2009; Ribolini et al., 2018; Gromig et al., 2018; Ruszkiczay-Rüdiger et al., 2020). Accordingly, this sample is considered as a young outlier due to post-depositional erosion or boulder toppling (Balco, 2011; Heyman et al., 2011). The remaining four samples are still largely scattered and manifest a strong bias towards old ages, which prevented us from fitting a PDF to this sample set (Fig. 11C). Three out of four CRE ages suggest LGM or earliest Lateglacial ages, relevant for Units 1 and 2, and thus violating the morphostratigraphically-based presumption that moraines belonging to a shrinking glacier should provide progressively younger ages in less extended glacial phases. Accordingly, the  $^{10}\text{Be}$  concentrations of these boulders were most probably increased by an inherited CRN inventory, leading to older apparent exposure ages compared to the timing of moraine stabilization (Briner et al., 2016; Crest et al., 2017; Ruszkiczay-Rüdiger et al., 2021a). Therefore, following the approach of Applegate et al. (2012) and Ruszkiczay-Rüdiger et al. (2021a), the morphostratigraphically coherent youngest age of  $15.2 \pm 1.4$  ka can be accepted as the best estimate of the maximum age of this landform. Nonetheless, in case this boulder has also arrived with certain amount of inherited  $^{10}\text{Be}$ , this apparent exposure age is still older than the true age of moraine stabilization.

### 5.2. The timing of the maximum ice extent in the Balkan Peninsula

U-series data of secondary carbonates cementing moraines provided  $>350$  ka for the MIE in Montenegro (Orjen and Durmitor Mts; Hughes et al., 2010, 2011) and in Greece (Pindus; Hughes et al., 2006a,b). The same method on piedmont outwash sediments provided  $>210$  ka at Mt. Olympus (Smith et al., 2006). These results are placing the MIE to the MIS 12 or 8.

The  $^{10}\text{Be}$  exposure age of the local MIE in the Jakupica Mts coincided with the LGM, similarly to Šar Mts (Kuhlemann et al., 2009) and Rila Mts (Kuhlemann et al., 2013a). This timing is also in agreement with some recently  $^{36}\text{Cl}$  dated landforms of the maximum ice extent in the Dinarides (Vran and Čvrnsnica Mts, Çiner et al., 2019; Southern Velebit Mt., Sarikaya et al., 2020). In Mt Chelmos in Greece and in the Northern Velebit Mt. in the Dinarides, however, the MIE was dated by  $^{36}\text{Cl}$  to earlier part of the late Pleistocene (MIS 4) (Pope et al., 2017; Žebre et al., 2021). On the contrary, in some Dinaric ranges  $^{36}\text{Cl}$  data placed the MIE moraines to the latest Pleistocene cooling phases: to the Oldest Dryas ( $\sim 15$  ka; Velež) and to the Younger Dryas ( $\sim 12$  ka, Crvanj) (Žebre et al., 2019).

This diachronous nature of the glacier maxima is characteristic not only to the Balkan Peninsula, but throughout the entire Mediterranean (Allard et al., 2021). Apparently, there is a methodological bias in the determined age of the maximum ice extent in the Balkan Peninsula. Each dating method has its advantage and drawback, which has to be

considered when interpreting the data in a regional picture. The pedogenic secondary carbonates might behave as open system, and thus the apparent ages might be older than the real age due to U leaching from the system (Richards and Dorale, 2003). The reliability of CRN dating largely depends on the accuracy of production rates and estimates of surface denudation rates. These issues are rather well resolved for  $^{10}\text{Be}$ , as extensive calibration work during the last decade made its production rate well constrained (Borchers et al., 2016), and it is produced in quartz-rich lithologies where the surface denudation rate is usually limited (Balco, 2011). However, the uncertainties for the production rate of  $^{36}\text{Cl}$  in Ca are higher (Schimmelpennig et al., 2009, 2011; Braucher et al., 2011; Marrero et al., 2016), and estimates of limestone denudation rates between 0.6 and 100 mm/ka are widely variable (Krklec et al., 2021). Long-term measurements of limestone denudation rates using in situ produced cosmogenic  $^{36}\text{Cl}$  studies from the Mediterranean area mostly provide denudation rates between 20 and 60 mm/ka, with slight dependence of slope convexity, but with a limited effect of climatic factors (Matsushi et al., 2010; Zerathe et al., 2013; Merchel et al., 2014; Godard et al., 2016; Thomas et al., 2017; Krklec et al., 2018). The user-defined surface denudation rate in the regional studies varies from 0 to 40 mm/kyr. The evaluation of these discrepancies is beyond the scope of the present study, and thus the published data are referenced and discussed here as interpreted in the original studies.

Nevertheless, it is of crucial importance to keep in mind that the above described uncertainties of limestone denudation rates can lead to twofold or even threefold changes of the published  $^{36}\text{Cl}$  exposure ages. In a more extreme case, if faster denudation rates are considered to be valid, the surface may be in steady state and the  $^{36}\text{Cl}$  concentrations should be interpreted as denudation rates instead of exposure ages. For instance, some  $^{36}\text{Cl}$  exposure durations on the Mt Chelmos published considering zero denudation rates (Pope et al., 2017), would be much older or in steady state if recalculated by 40 mm/ka limestone denudation rates considered at several locations in the Dinarides (Vran and Čvrnsnica Mts - Çiner et al., 2019; Velez and Crvanj Mts - Žebre et al., 2019). Accordingly, although the  $^{36}\text{Cl}$  glacier chronologies opened new opportunities of age determination of past glacial phases in carbonate areas, data must be considered with caution, as it was also stressed by previous authors (Sarikaya et al., 2020, Žebre et al., 2021).

### 5.3. Regional trends of equilibrium line altitudes during the LGM

As the MIE glaciers do not represent the same horizon in time, in this section we aim at a comparison of the ELAs of the glaciers dated to the LGM. The recalculation of all the cited ELAs using the same method is out of the scope of this study, hence, published ELAs are discussed as originally provided, regardless of the method used for their calculation.

First, the relationship between the ELAs and the distance from the Adriatic coast was examined. For this purpose, the Adriatic coast with a sea level 120 m lower than the present day-sea level was considered, as suggested for the LGM (Spratt and Lisiecki, 2016; Zickel et al., 2016; Fig. 1C). The distance from the Adriatic coast was measured as the shortest straight line between the central part of the mountain range and the closest point of the coastline (Table S5).

Interestingly the lowest LGM ELA was reported from the Southern Velebit Mt ( $\sim 1300$  m; Bognar and Faivre, 2006; Sarikaya, et al., 2020), currently being at  $\sim 7$  km distance from the Adriatic coast, but it was at  $\sim 70$  km away from the LGM coastline. The second lowest value ( $\sim 1456$  m) was reported for in the Orjen Mt (Hughes et al. 2010), at  $\sim 16$ – $18$  km distance from the coast currently and during the LGM as well. Other ELA values in the Central Balkan Peninsula show a steady rise with increasing distance from the sea. The highest values are estimated for the Jakupica and Šar Mts with ELAs close to or somewhat above  $\sim 2100$  m at a distance of  $\sim 120$ – $130$  km from the LGM coast (Table S5 and references therein, Fig. 12).

Another interesting feature is that the Rila Mt, located at a distance of  $\sim 340$  km from the coast, has its mean ELA at  $2150 \pm 120$  m asl,

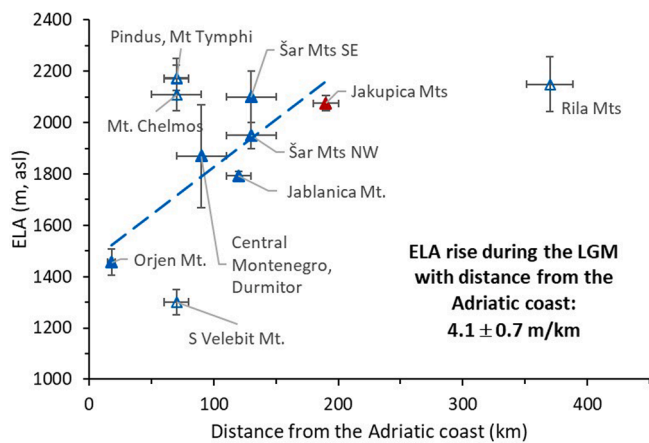


**Fig. 12.** LGM ELAs plotted against the mean distance from the Adriatic coast at 120 m lower sea level than today, as suggested for the LGM (Spratt and Lisiecki, 2016; Zickel et al., 2016) of the mountain ranges where relevant data are available. Open triangles are data omitted from the linear regression. Red triangle is the study area. For data and references refer to the text and Table S5.

suggesting that this increasing trend is valid within a distance of 150–200 km from the coast; further inland the ELA is apparently not rising anymore.

In the southern part of the Balkan Peninsula, the LGM ELAs appear to be at higher elevation with respect to their distance from the Adriatic coast than in its central part, with ELAs above 2100 m at only ~70 km from the western shoreline (Table S5 and references therein, Fig. 12).

In order to find the best fit rate for the rise of the ELA with the distance from the Adriatic Sea in the central Balkan Peninsula, a linear, least-squares fitting was applied (Williamson-York bivariate fitting; Cantrell, 2008). The outlying data representing the southern part of the Peninsula (Pindus, Chelmos) and the inland Rila Mts, together with the Southern Velebit Mts of exceptionally low ELA, were excluded from this calculation.

The mountains in the southern part of the peninsula were apparently drier than expected considering their high ELAs and relatively short distance from the coast, while the inland Rila Mts must have received more precipitation than it would be expected (Fig. 12). This implies that the NE part of the Balkan Peninsula might have received more moisture from the westerlies prevailing in the inland areas (Ruzkiczay-Rüdiger et al., 2009; Mîndrescu et al., 2010; Sebe et al., 2011, 2015; Zasadni et al., 2021; Klapýta et al., 2022a, b) than it was suggested before (Kuhlemann et al., 2013a), explaining the observed ceasing of the ELA increase. However, further glacio-climatological studies will be necessary to better constrain the inland changes of the ELA values in the area.

The exceptionally high moisture in the Southern Velebit Mt. suggested by its low, ~1300 m ELA value at a relatively larger distance from the LGM Adriatic coastline still needs further exploration. It is interesting to note that this ELA is close to the MIE ELAs reported for other coastal ranges, however dated to older Pleistocene glaciations (Northern Velebit Mt.,  $1364 \pm 51$  m, Žebre et al., 2021; Orjen Mt., ~1256 m, Hughes et al., 2010; and Lovćen, ~1259 m, Žebre and Stepišnik, 2014), proposing the need for further numerical age determination of the glacial landforms.

The trendline fitted to the statistically coherent dataset from the Central Balkan Peninsula gives an ELA rise of  $\sim 4.1 \pm 0.7$  m/km ( $r^2 = 0.8$ ) (Fig. 12); a value slightly lower than the  $\sim 5.4$  m/km calculated for the LGM and 6.4 m/km for the MIE glaciers in the Orjen and Durmitor Mts (Hughes et al., 2011).

The characteristic increase of the ELAs from the Adriatic coast towards the inland areas is indicative of a precipitation supply from the south in the Central Balkan Peninsula during the LGM. This is in agreement with previous glacio-climatological models suggesting that

during the LGM a dominantly southerly circulation was prevailing to the south of the European Alps (Florineth and Schlüchter, 2000; Kuhlemann et al., 2008; Becker et al., 2016). This might have been facilitated by major temperature contrasts between the European landmass and the Mediterranean Sea, sustaining lee-side vortices to the south of the Alps, in the Gulf of Genoa and Adriatic Sea, forming weak moisture-bearing depressions providing excess precipitation along the northern Mediterranean coast and drier conditions inland (Hughes et al., 2010). The decreased precipitation in the inland areas is reflected also by extensive loess deposition (Obrecht et al., 2019; Lehmkuhl et al., 2021). To the north, in the Pannonian Basin and the Carpathians, apparently the zonal, westerly winds were dominant, similarly to the present day pattern, as it is inferred from landforms of aeolian erosion in the basin interior (Ruzkiczay-Rüdiger et al., 2007, 2009; Sebe et al., 2011, 2015) and of glacial erosion in the Carpathians (Mîndrescu et al., 2010; Zasadni et al., 2018, 2021; Klapýta et al., 2021a,b, 2022b).

#### 5.4. Glacio-climatological modelling

Constraining the degree-day model with the regional estimate of the global pollen-based cooling of the warmest month ( $T_{\text{July}}$  drop:  $\sim 8^\circ\text{C}$ ; Cleator et al., 2020) and the current annual temperature range, provides an inferred MAAT drop of 6–7 °C (Fig. 10, Table S4). Regional estimates derived from a recent paleoclimate data assimilation (Tierney et al., 2020) also suggest a 6 to 7 °C drop in MAAT during the LGM for North Macedonia. The groundwater noble gas temperature data from a recent global recalculation campaign (Seltzer et al., 2021) provided slightly larger cooling ( $\sim 9.2^\circ\text{C}$ ) at northern (Varsányi et al., 2011) and slightly lower cooling ( $\sim 5.4^\circ\text{C}$ ) at southern latitudes (Abouelmagd et al., 2014), also implying 6 to 7 °C drop in mean annual temperature during the LGM for study area. Taking this drop of the inferred MAAT and the current annual temperature range,  $\sim 1.5$  times more LGM accumulation would have been required compared to the current MAP to maintain the reconstructed paleoglaciers in the Jakupica Mts (Fig. 10, Table S4). Glacio-climatological modelling using the recent temperature range in a coastal massif in Montenegro also suggested a slight decrease of the modelled precipitation at 6 to 7 °C MAAT depression (Hughes et al., 2010).

In case the model is constrained with the increased annual temperature range suggested by the pollen-based estimate at  $\sim 21$  ka (Cleator et al., 2020), the simulated annual melt gets closer to the current annual precipitation sum, although still implies wetter conditions ( $\sim 1.3$  times more precipitation) compared to the current climate (Fig. 10, Table S4). In this case, the MAAT drop of  $\sim 11^\circ\text{C}$  inferred from the degree-day model agrees fairly well the pollen-based estimate of LGM MAAT drop in the Jakupica Mts ( $\sim 10.88^\circ\text{C}$ ; Cleator et al., 2020). This degree of cooling is larger than estimated by a recent paleoclimate data assimilation (Tierney et al., 2020). However, if the increased annual temperature range was considered for a 6 to 7 °C drop in MAAT, an extremely high accumulation surplus ( $\sim 3.5$  times more precipitation) is modelled, rendering this scenario unrealistic for the Jakupica Mts (Fig. 10, Table S4).

Considering both the current and increased temperature range models, the hydroclimate estimates are still in contrast with the pollen-based estimate of MAP (Cleator et al., 2020). This indicates  $\sim 42\%$  (from 36% to 47%) precipitation decrease during the LGM compared to the current MAP in the Jakupica Mts (Fig. 10). A recent study argued that traditional pollen-based paleoclimate methods passing over the plant physiological effects of atmospheric  $\text{CO}_2$  are prone to a dry bias in glacial conditions with typically low  $\text{CO}_2$  (Prentice et al., 2022). This bias can partially explain the mismatch and support the credit of the wetter glacio-climatological reconstructions in the Jakupica Mts. The wetter LGM conditions inferred from the degree-day model contrasting the pollen-based estimates of drier LGM, support the criticism on neglecting the negative effect of low  $\text{CO}_2$  on plant water-use efficiency and the overestimation of the dryness of glacial intervals based on the

pollen spectra using traditional (statistical or modern-analogue) approaches (Prentice et al., 2022). The results of the degree-day modelling suggest wetter than today, or similarly wet, LGM conditions in the Jakupica Mts, and thus support those paleoclimate model variants, which argue for an increased precipitation during the LGM in this region (Ludwig et al., 2016).

## 6. Conclusions

Geomorphological mapping allowed to reconstruct the ice extent of the local glacial maximum and five phases of deglaciation in the Jakupica Mts.  $^{10}\text{Be}$  CRE age determination was successful for the moraines of the two phases of largest glacier extent: the local MIE was dated to the late part of the LGM (~19.3 ka), which was followed by a short phase of glacier recession and glacier stabilization during the beginning of the Lateglacial (~18.2 ka). These results are in agreement with other studies placing the MIE to the LGM in the Balkan Peninsula, while they are in apparent contradiction with studies suggesting that the MIE occurred during an earlier glacial phase. Further geochronological research is needed to decide whether the age discrepancies reflect methodological problems of age determination or a real asynchronous timing of the MIE in the area.

Unfortunately, the presence of inherited CRN inventory hindered the age determination of the final deglaciation of the range. The LGM ELA of the reconstructed glaciers (~2070 m asl) fits well within the regional trend pointing to an inland increase of the ELAs.

Glacio-climatological modelling was performed for the MIE, assigned to the LGM by the  $^{10}\text{Be}$  exposure age data. Our model, constrained by the geomorphological evidence and by the July temperature drop suggested by pollen-based paleoclimate reconstructions, points to similar or wetter conditions during the LGM with respect to present day values. These relatively wet LGM climate conditions, however, contrast with the pollen-based hydroclimate in the Jakupica Mts and support the existence of a dry bias during glacial phases in former pollen-inferred paleoclimate reconstructions, which neglect the negative effect of low  $\text{CO}_2$  on plant physiology. The results of the degree-day model, indicating wetter (or similar to modern) conditions in the Jakupica Mts, are in agreement with paleoclimate models, which predict increased southerly moisture advection in the central Balkan Peninsula during the Pleistocene glaciations.

## Declaration of Competing Interest

The authors declare that they have no known competing financial interests or personal relationships that could have appeared to influence the work reported in this paper.

## Acknowledgements

This research was funded by the National Research, Development and Innovation Office of Hungary grant FK 124807, co-financed by the European Regional Development Fund in the project of GINOP-2.3.2-15-2016-00009 'ICER'. AMS measurements at VERA were covered by the Radiate Transnational Access grant 19001688-ST under the Grant Agreement 824096 from the EU Research and Innovation programme HORIZON 2020. Fieldwork was carried out under Research Permit No. UP1-11/1-422/2018 issued by the Ministry of Environment and Physical Planning of the Republic of Macedonia. This is contribution No. 80 of the 2 ka Paleoclimatology Research Group. Ivett Kovács is acknowledged for the quality control of pure quartz samples by X-ray diffraction measurements. We are thankful to Silke Merchel for her contribution to the AMS measurements. We are indebted to Jerzy Zasadni and an Anonymous Reviewer for their comments and suggestions that helped a lot to improve the manuscript.

## Appendix A. Supplementary data

Supplementary data to this article can be found online at <https://doi.org/10.1016/j.catena.2022.106383>.

## References

- Abouelmagd, A., Sultan, M., Sturchio, N. C., Soliman, F., Rashed, M., Ahmed, M., Kehew, A.E., Milewski, A., Chouinard, K. 2014. Paleoclimate record in the Nubian sandstone aquifer, Sinai Peninsula, Egypt. *Quat. Res.* 81(1), 158–167.
- Allard, J.L., Hughes, P.D., Woodward, J.C., 2021. A radiometric dating revolution and the Quaternary glacial history of the Mediterranean mountains. *Earth Sci. Rev.* 223, 10384.
- Akhmadaliev, S., Heller, R., Hanf, D., Rugel, G., Merchel, S., 2013. The new 6 MV AMS-facility DREAMS at Dresden. *Nucl. Instr. Meth. B* 294, 5–10.
- Applegate, P.J., Urban, N.M., Keller, K., Lowell, T.V., Laabs, B.J.C., Kelly, M.A., Alley, R. B., 2012. Improved moraine age interpretations through explicit matching of geomorphic process models to cosmogenic nuclide measurements from single landforms. *Quat. Res.* 77 (2), 293–304.
- Arsovski, M., 1997. Tektonika na Makedonija. *Rudarsko-Geol. Fak, Štip*, p. 306.
- Balco, G., 2009. MATLAB Code for Camel Diagrams. <http://cosmognosis.wordpress.com/2009/07/13/matlab-code-for-camel-diagrams> (February 2013).
- Balco, G., 2011. Contributions and unrealized potential contributions of cosmogenic-nuclide exposure dating to glacier chronology, 1990–2010. *Quaternary Science Reviews* 30 (1–2), 3–27.
- Balco, G., 2020. Glacier Change and Paleoclimate Applications of Cosmogenic-Nuclide Exposure Dating. *Annu. Rev. of Earth and Planet. Sci.* 48 (1), 21–48.
- Barr, I.D., Spagnolo, M., 2015. Glacial cirques as palaeoenvironmental indicators: Their potential and limitations. *Earth Sci. Rev.* 151, 48–78.
- Becker, P., Seguinot, J., Jouvét, G., Funk, M., 2016. Last Glacial Maximum precipitation pattern in the Alps inferred from glacier modelling. *Geogr. Helv.* 71, 173–187.
- Benn, D.I., Hulton, N.R.J., 2010. An Excel™ spreadsheet program for reconstructing the surface profile of former mountain glaciers and ice caps. *Comput. Geosci.* 36 (5), 605–610.
- Bognar, A., Faivre, S., 2006. Geomorphological traces of the younger Pleistocene glaciation in the central part of the Velebit Mt. *Hrvatski. Geografski Glasnik* 68 (02), 19–30.
- Borchers, B., Marrero, S., Balco, G., Caffee, M., Goehring, B., Lifton, N., Nishiizumi, K., Phillips, F., Schaefer, J., Stone, J., 2016. Geological calibration of spallation production rates in the CRONUS-Earth project. *Quat. Geochronol.* 31, 188–198.
- Braithwaite, R.J., 2008. Temperature and precipitation climate at the equilibrium line altitude of glaciers expressed by the degree-day factor for melting snow. *J. Glaciol.* 54 (186), 437–444.
- Braucher, R., Merchel, S., Borgomano, J., Bourlès, D.L., 2011. Production of cosmogenic radionuclides at great depth: A multi element approach. *Earth Planet. Sci. Lett.* 309 (1–2), 1–9.
- Briner, J.P., Goehring, B.M., Mangerud, J., Svendsen, J.I., 2016. The deep accumulation of  $^{10}\text{Be}$  at Utsira, southwestern Norway: implications for cosmogenic nuclide exposure dating in peripheral ice sheet landscapes. *Geophys. Res. Lett.* 43 (17), 9121–9129.
- Brown, E.T., Edmond, J.M., Raisbeck, G.M., Yiou, F., Kurz, M.D., Brook, E.J., 1991. Examination of surface exposure ages of Antarctic moraines using in situ produced  $^{10}\text{Be}$  and  $^{26}\text{Al}$ . *Geochimica et Cosmochimica Acta* 55 (8), 2269–2283.
- Brugger, K.A., 2006. Late Pleistocene climate inferred from the reconstruction of the Taylor River glacier complex, southern Sawatch Range, Colorado. *Geomorphology* 75 (3–4), 318–329.
- Cantrell, C.A., 2008. Technical Note: Review of methods for linear least-squares fitting of data and application to atmospheric chemistry problems. *Atmos. Chem. Phys.* 8, 5477–5487.
- Chmieleff, J., von Blanckenburg, F., Kossert, K., Jakob, D., 2010. Determination of the  $^{10}\text{Be}$  half-life by multicollector ICP-MS and liquid scintillation counting. *Nuclear Instruments & Methods in Physics Research, Section B, Beam Interactions with Materials and Atoms* 268 (2), 192–199.
- Çiner, A., Sarıkaya, M.A., Yıldırım, C., 2017. Misleading old age on a young landform? The dilemma of cosmogenic inheritance in surface exposure dating: moraines vs. rock glaciers. *Quat. Geochronol.* 42, 76–88.
- Çiner, A., Stepišnik, U., Sarıkaya, M.A., Zebre, M., Yıldırım, C., 2019. Last Glacial Maximum and Younger Dryas piedmont glaciations in Blidinje, the Dinaric Mountains (Bosnia and Herzegovina): insights from  $^{36}\text{Cl}$  cosmogenic dating. *Mediterr. Geosci. Rev.* 1 (1), 25–43.
- Cleator, S.F., Harrison, S.P., Nichols, N.K., Prentice, I.C., Roulstone, I., 2020. A new multivariable benchmark for Last Glacial Maximum climate simulations. *Climate of the Past* 16 (2), 699–712.
- Cowton, T., Hughes, P.D., Gibbard, P.L., 2009. Palaeoglaciation of Parque Natural Lago de Sanabria, northwest Spain. *Geomorphology* 108 (3–4), 282–291.
- Crest, Y., Delmas, M., Braucher, R., Gunnell, Y., Calvet, M., 2017. Cirques have growth spurts during deglacial and interglacial periods: Evidence from  $^{10}\text{Be}$  and  $^{26}\text{Al}$  nuclide inventories in the central and eastern Pyrenees. *Geomorphology* 278, 60–77.
- Cvijić, J., 1898. Das Rilagebirge und seine ehemalige Vergletscherung. *Zeitschrift der Gesellschaft für Erdkunde zu Berlin* 33.
- Cvijić, J., 1917. L'époque glaciaire dans la péninsule des Balkans. *Annales de Géographie* 141, 189–218.
- Dedijer, J., 1917. Traces glaciaires en Albanie et en Nouvelle Serbie. *La Géographie - Bulletin de la Société de Géographie* 31, 325–337.

- Dumurdžanov, N., Stojanov, R., Petrovski, K., 1979. Explanatory Notes for the General Geological Map of Kruševo, 1:100 000. Belgrade, Federal Geological Survey, p. 58.
- Dumurdžanov, N., Serafimovski, T., Burchfiel, B.C., 2004. Evolution of the Neogene-Pleistocene basins of Macedonia. *Geol. Soc. Am. Digit. Map Chart* 1, 1–20.
- Florineth, D., Schlüchter, C., 2000. Alpine evidence for atmospheric circulation patterns in Europe during the Last Glacial Maximum. *Quat. Res.* 54 (3), 295–308.
- Godard, V., Ollivier, V., Bellier, O., Miramont, C., Shabanian, E., Fleury, J., Benedetti, L., Guillou, V., 2016. Weathering-limited hillslope evolution in carbonate landscapes. *Earth Planet. Sci. Lett.* 446, 10–20.
- Golledge, N., Hubbard, A., Bradwell, T., 2010. Influence of seasonality on glacier mass balance, and implications for palaeoclimate reconstructions. *Climate Dynamics* 35 (5), 757–770.
- Gosse, J.C., Phillips, F.M., 2001. Terrestrial in situ cosmogenic nuclides: theory and application. *Quat. Sci. Rev.* 20 (14), 1475–1560.
- Gripp, K., 1922. Beiträge zur Geologie von Mazedonien. *Hamburg. Univ. Abh. a.d. Gebiet d. Auslands*, Bd. 7, Reihe C. Natur., Bd. 3, Hamburg, 61 p.
- Gromig, R., Mechemich, S., Ribolini, A., Wagner, B., Zanchetta, G., Isola, I., Bini, M., Dunai, T., 2018. Evidence for a Younger Dryas deglaciation in the Galicica Mountains (FYROM) from cosmogenic  $^{36}\text{Cl}$ . *Quat. Int.* 464, 352–363.
- Heyman, J., Stroeven, A.P., Harbor, J.M., Caffee, M.W., 2011. Too young or too old: evaluating cosmogenic exposure dating based on an analysis of compiled boulder exposure ages. *Earth Planet. Sci. Lett.* 302 (1–2), 71–80.
- Hughes, P.D., Gibbard, P.L., Woodward, J.C., 2005. A Formal stratigraphical approach for Quaternary glacial records in mountain regions. *Episodes* 28, 85–92.
- Hughes, P.D., Woodward, J.C., Gibbard, P.L., Macklin, M.G., Gilmour, M.A., Smith, G.R., 2006a. The glacial history of the Pindus Mountains. *Greece. J. Geol.* 114 (4), 413–434.
- Hughes, P., Woodward, J., Gibbard, P., 2006b. Late Pleistocene glaciers and climate in the Mediterranean. *Glob. Planet. Chang.* 50 (1–2), 83–98.
- Hughes, P.D., Braithwaite, R.J., 2008. Application of a degree-day model to reconstruct Pleistocene glacial climates. *Quat. Res.* 69 (1), 110–116.
- Hughes, P.D., Woodward, J.C., van Calsteren, P.C., Thomas, L.E., Adamson, K.R., 2010. Pleistocene ice caps on the coastal mountains of the Adriatic Sea: palaeoclimatic and wider palaeoenvironmental implications. *Quat. Sci. Rev.* 29 (27–28), 3690–3708.
- Hughes, P.D., Woodward, J.C., van Calsteren, P.C., Thomas, L.E., 2011. The glacial history of the Dinaric Alps. *Montenegro. Quat. Sci. Rev.* 30 (23–24), 3393–3412.
- Isola, I., Ribolini, A., Bini, M., Zanchetta, G., Milevski, I., 2021. Geomorphology of the topmost part of the Bistra Mountain, Mavrovo Park. *North Macedonia. J. of Maps* 17 (2), 401–412.
- Jancevski, J., Golbov, K., Temkova, V., 1984. Explanatory Notes for the General Geological Map of Skopje, 1:100 000. Federal Geological Survey, Belgrade, p. p. 57.
- Jovanović, P.S., 1928. Glacijacija Jakupice. Posebna izdanja Srpskog Geografskog Društva 4, 1–86 in Serbian.
- Klapyta, P., Mîndrescu, M., Zasadni, J., 2021a. Geomorphological record and equilibrium line altitude of glaciers during the last glacial maximum in the Rodna Mountains (eastern Carpathians). *Quat. Res.* 100, 1–20.
- Klapyta, P., Zasadni, J., Dubis, L., Świąder, A., 2021b. Glaciation in the highest parts of the Ukrainian Carpathians (Chornohora and Svydovets massifs) during the local last glacial maximum. *Catena* 203, 105346.
- Klapyta, P., Bryndza, M., Zasadni, J., Jasionek, M., 2022a. The lowest elevation Pleistocene glaciers in the Carpathians—The geomorphological and sedimentological record of glaciation in the Polonyna Rivna and Borzhava massifs (Ukraine Carpathians). *Geomorphology* 398, 108060.
- Klapyta, P., Mîndrescu, M., Zasadni, J., 2022b. The impact of local topoclimatic factors on marginal Pleistocene glaciation in the Northern Romanian Carpathians. *Catena* 210, 105873.
- Kolčakovski, D., 1988. Visokoplaninski karst na planinatu Karadžica. *Geogr. Rev.* 26, 95–113.
- Korschinek, G., Bergmaier, A., Faestermann, T., Gerstmann, U.C., Knief, K., Rugel, G., Wallner, A., Dillmann, I., Dollinger, G., von Gossmi, C.L., Kossert, K., Maiti, M., Poutivtsev, M., Remmert, A., 2010. A new value for the half-life of  $^{10}\text{Be}$  by heavy-ion elastic recoil detection and liquid scintillation counting. *Nuclear Instruments & Methods in Physics Research, Section B, Beam Interactions with Materials and Atoms* 268 (2), 187–191.
- Krklec, K., Domínguez-Villar, D., Perica, D., 2015. Depositional environments and diagenesis of a carbonate till from a Quaternary paleoglacier sequence in the Southern Velebit Mountain (Croatia). *Palaeogeogr. Palaeoclimatol. Palaeoecol.* 436, 188–198.
- Krklec, K., Domínguez-Villar, D., Braucher, R., Perica, D., Mrak, I., 2018. Morphometric comparison of weathering features on side by side carbonate rock surfaces with different exposure ages – a case from the Croatian coast. *Quat. Int.* 494, 275–285.
- Krklec, K., Domínguez-Villar, D., Perica, D., 2021. Use of rock tablet method to measure rock weathering and landscape denudation. *Earth Sci. Rev.* 212, 103449.
- Kuhlemann, J., Rohling, E.J., Krumrei, I., Kubik, P., Ivy-Ochs, S., Kucera, M., 2008. Regional synthesis of Mediterranean atmospheric circulation during the last glacial maximum. *Sci.* 321, 1338–1340.
- Kuhlemann, J., Milivojević, M., Krumrei, I., Kubik, P.W., 2009. Last glaciation of the Sara range (Balkan peninsula): Increasing dryness from the LGM to the Holocene. *Austrian J. Earth Sci.* 102, 146–158.
- Kuhlemann, J., Gachev, E., Gikov, A., Nedkov, S., Krumrei, I., Kubik, P., 2013a. Glaciation in the Rila mountains (Bulgaria) during the Last Glacial Maximum. *Quat. Int.* 293, 51–62.
- Kuhlemann, J., Dobre, F., Urdea, P., Krumrei, I., Gachev, E., Kubik, P., Rahn, M., 2013b. Last glacial maximum glaciation of the central South-Carpathian Range (Romania). *Austrian J. Earth Sci.* 106, 50–62.
- Lal, D., 1991. Cosmic-ray labelling of erosion surfaces e in-situ nuclide production rates and erosion models. *Earth Planet. Sci. Lett.* 104, 424–439.
- Lazarevski, A., 1993. Climate of Macedonia. *Kultura, Skopje in Macedonian.*
- Lehmkuhl, F., Nett, J.J., Pötter, S., Schulte, P., Sprafke, T., Jary, Z., Antoine, P., Wacha, L., Wolf, D., Zerbini, A., Hošek, J., Marković, S.B., Obrecht, I., Sümege, P., Veres, D., Zeeden, C., Boemke, B., Schaubert, V., ... Hambach, U., 2021. Loess landscapes of Europe—Mapping, geomorphology, and zonal differentiation. *Earth Sci. Rev.* 215, 103496.
- Leontaritis, A.D., Kouli, K., Pavlopoulos, K., 2020. The glacial history of Greece: a comprehensive review. *Mediterr. Geosci. Rev.* 2 (1), 65–90.
- Lifton, N.A., Sato, T., Dunai, T.J., 2014. Scaling in situ cosmogenic nuclide production rates using analytical approximations to atmospheric cosmic-ray fluxes. *Earth Planet. Sci. Lett.* 386, 149–160.
- Lifton, N.A., 2016. Implications of two Holocene time-dependent geomagnetic models for cosmogenic nuclide production rate scaling. *Earth Planet. Sci. Lett.* 433, 257–268.
- Lisiecki, L.E., Raymo, M.E., 2005. A Pliocene-Pleistocene stack of 57 globally distributed benthic  $\delta^{18}\text{O}$  records. *Paleoceanography* 20 (1), n/a–n/a.
- Ludwig, P., Schaffernicht, E.J., Shao, Y., Pinto, J., G., 2016. Regional atmospheric circulation over Europe during the Last Glacial Maximum and its links to precipitation. *J. Geophys. Res. Atmos.* 121, 2130–2145.
- Manakovik, D., 1966. Nekoi reljefni elementi vo poročieto na Babuna i Topolka so Titoveškatata kotlina. *Godišen Zbornik, Geografski Institut Skopje* 15, 87–139.
- Marrero, S.M., Phillips, F.M., Caffee, M.W., Gosse, J.C., 2016. CRONUS-Earth cosmogenic  $^{36}\text{Cl}$  calibration. *Quat. Geochronol.* 31, 199–219.
- Matsushi, Y., Sasa, K., Takahashi, T., Sueki, K., Nagashima, Y., Matsukura, Y., 2010. Denudation rates of carbonate pinnacles in Japanese karst areas: Estimates from cosmogenic  $^{36}\text{Cl}$  in calcite. *Nuclear Instruments and Methods in Physics Research Section B: Beam Interactions with Materials and Atoms* 268, 1205–1208.
- Merchel, S., Hergers, U., 1999. An Update on Radiochemical Separation Techniques for the Determination of Long-Lived Radionuclides via Accelerator Mass Spectrometry. *Radiochim. Acta* 84, 215–219.
- Merchel, S., Mrak, I., Braucher, R., Benedetti, L., Repe, B., Bourlès, D.L., Reiter, J.M., 2014. Surface exposure dating of the Veliki vrh rock avalanche in Slovenia associated with the 1348 earthquake. *Quat. Geochronol.* 22, 33–42.
- Merchel, S., Gärtner, A., Beutner, S., Bookhagen, B., Chabilan, A., 2019. Attempts to understand potential deficiencies in chemical procedures for AMS: Cleaning and dissolving quartz for  $^{10}\text{Be}$  and  $^{26}\text{Al}$  analysis. *Nuclear Instruments and Methods in Physics Research Section B: Beam Interactions with Materials and Atoms* 455, 293–299.
- Milevski, I., Gorin, S., Markoski, M., Radevski, I., 2013. Comparison of Accuracy of DEM's Available for the Republic of Macedonia. *Proceedings from the 3<sup>rd</sup> International Geographic Symposium*.
- Milevski, I., Radevski, I., Dimitrovska, O., Svemir, G., 2015. Digital model of the mean annual temperature and precipitation in Macedonia. *Geogr. Rev.* 48, 27–34.
- Milojević, B.Z., 1937. Visoke planine u našoj Kraljevini. *Državna štamparija Kraljevine Jugoslavije, Beograd.*
- Mîndrescu, M., Evans, I.S., Cox, N.J., 2010. Climatic implications of cirque distribution in the Romanian Carpathians: palaeowind directions during glacial periods. *J. Quat. Sci.* 25 (6), 875–888.
- Nishizumi, K., Imamura, M., Caffee, M.W., Southon, J.R., Finkel, R.C., McAninch, J., 2007. Absolute calibration of  $^{10}\text{Be}$  AMS standards. *Nuclear Instruments and Methods in Physics Research Section B: Beam Interactions with Materials and Atoms* 258 (2), 403–413.
- Nye, J.F., 1952. The mechanics of glacier flow. *J. Glaciol.* 2 (12), 82–93.
- Obrecht, I., Zeeden, C., Hambach, U., Veres, D., Marković, S.B., Lehmkuhl, F., 2019. A critical reevaluation of palaeoclimate proxy records from loess in the Carpathian Basin. *Earth Sci. Rev.* 190, 498–520.
- Oien, R.P., Rea, B.R., Spagnolo, M., Barr, I.D., Bingham, R.G., 2021. Testing the area-altitude balance ratio (AABR) and accumulation-area ratio (AAR) methods of calculating glacier equilibrium-line altitudes. *J. Glaciol.* 68 (268), 357–368.
- Oestreich, K., 1902. Beiträge zur geomorphologie Makedoniens. *K.K. geogr. Ges., Wien, Abh.* p. 93.
- Osmaston, H., 2005. Estimates of glacier equilibrium line altitudes by the Area×Altitude, the Area×Altitude Balance Ratio and the Area×Altitude Balance Index methods and their validation. *Quat. Int.* 138–139, 22–31.
- Palyvos, N., Sorel, D., Lemeille, F., Mancini, M., Pantosti, D., Julia, R., Triantaphyllou, M., De Martini, P.M., 2007. Review and new data on uplift rates at the W termination of the Corinth Rift and the NE Rion graben area (Achaia, NW Peloponnesos). *Bull. Geol. Soc. Greece* 40, 412–424.
- Peel, M.C., Finlayson, B.L., McMahon, T.A., 2007. Updated world map of the Köppen-Geiger climate classification. *Hydrol. Earth Syst. Sci.* 11, 1633–1644.
- Pellitero, R., Rea, B.R., Spagnolo, M., Bakke, J., Hughes, P., Ivy-Ochs, S., Lukas, S., Ribolini, A., 2015. A GIS tool for automatic calculation of glacier equilibrium-line altitudes. *Comput. Geosci.* 82, 55–62.
- Pellitero, R., Rea, B.R., Spagnolo, M., Bakke, J., Ivy-Ochs, S., Frew, C.R., Hughes, P., Ribolini, A., Lukas, S., Renssen, H., 2016. GLaRe, a GIS tool to reconstruct the 3D surface of palaeoglaciologists. *Comput. Geosci.* 94, 77–85.
- Pennos, C., Lauritzen, S.E., Vouvalidis, K., Cowie, P., Pechlivanidou, S., Gkarlaoui, C., Styllas, M., Tsourlos, P., Mouratidis, A., 2019. From subsurface to surface: a multidisciplinary approach to decoding uplift histories in tectonically-active karst landscapes. *Earth Surf. Process. Landf.* 44, 1710–1721.
- Petreska, B., 2008. Podzemni karstni formi vo Porečiot Basen i nivna valorizacija za potrebite na prostornoto planiranje. *Master Thesis. Faculty of Natural Science and Mathematics, Skopje.*

- Pope, R.J., Hughes, P.D., Skourtsos, E., 2017. Glacial history of Mt Chelmos, Peloponnesus, Greece. *Geological Society, London, Special Publications* 433 (1), 211–236.
- Prentice, I. C., Villegas-Diaz, R., Harrison, S. P., 2022. Accounting for atmospheric carbon dioxide variations in pollen-based reconstruction of past hydroclimates. *Global and Planet. Change*, 211, 103790.
- Rea, B.R., 2009. Defining modern day Area-Altitude Balance Ratios (AABRs) and their use in glacier-climate reconstructions. *Quat. Sci. Rev.* 28 (3-4), 237–248.
- Ribolini, A., Bini, M., Isola, I., Spagnolo, M., Zanchetta, G., Pellitero, R., Mechernich, S., Gromig, R., Dunai, T., Wagner, B., Milevski, I., 2018. An Oldest Dryas glacier expansion on Mount Pelister (Former Yugoslavian Republic of Macedonia) according to <sup>10</sup>Be cosmogenic dating. *J. Geol. Soc. Lond.* 175 (1), 100–110.
- Richards, D., Dorale, J., 2003. Uranium-series chronology and environmental applications of speleothems. *Rev. Mineral. Geochem.* 52, 407–460.
- Ruzsiczay-Rüdiger, Z., Fodor, L.I., Horváth, E., 2007. Neotectonics and Quaternary landscape evolution of the Gödöllő Hills, Central Pannonian Basin. Hungary. *Glob. Planet. Change* 58 (1-4), 181–196.
- Ruzsiczay-Rüdiger, Z., Fodor, L., Horváth, E., Telbisz, T., 2009. Discrimination of fluvial, eolian and neotectonic features in a low hilly landscape, a DEM-based morphotectonic analysis in the Central Pannonian Basin, Hungary. *Geomorphology* 104 (3-4), 203–217.
- Ruzsiczay-Rüdiger, Z., Kern, Z., Urdea, P., Braucher, R., Madarász, B., Schimmelpennig, I., 2016. Revised deglaciation history of the Pietrele-Stănișoara glacial complex, Retezat Mts, Southern Carpathians. Romania. *Quat. Int.* 415, 216–229.
- Ruzsiczay-Rüdiger, Zs., Kern, Z., Temovski, M., Madarász, B., Milevski, I., Braucher, R., ASTER Team, 2020. Last deglaciation in the central Balkan Peninsula: Geochronological evidence from Jablanica Mt. (North Macedonia). *Geomorphology* 351, 106985.
- Ruzsiczay-Rüdiger, Z., Kern, Z., Urdea, P., Madarász, B., Braucher, R., ASTER Team, 2021a. Limited glacial erosion during the last glaciation in mid-latitude cirques (Retezat Mts, Southern Carpathians, Romania). *Geomorphology* 384, 107719.
- Ruzsiczay-Rüdiger, Z., Neuhuber, S., Braucher, R., Lachner, J., Steier, P., Wieser, A., Braun, M., Bourlès, D., Aumaître, G., Keddadouché, K., 2021b. Comparison and performance of two cosmogenic nuclide sample preparation procedures of in situ produced <sup>10</sup>Be and <sup>26</sup>Al. *J. Radioanal. Nucl. Chem.* 329 (3), 1523–1536.
- Sarikaya, M.A., Stepišnik, U., Žebre, M., Çiner, A., Yıldırım, C., Vlahović, I., Tomljenović, B., Matoš, B., Wilken, K.M., 2020. Last glacial maximum deglaciation of the Southern Velebit Mt. (Croatia): insights from cosmogenic <sup>36</sup>Cl dating of Rujanska Kosa. *Mediterr. Geosci. Rev.* 2 (1), 53–64.
- Schimmelpennig, I., Benedetti, L., Finkel, R., Pik, R., Blard, P.-H., Bourlès, D., Burnard, P., Williams, A., 2009. Sources of in-situ <sup>36</sup>Cl in basaltic rocks. Implications for calibration of production rates. *Quat. Geochronol.* 4 (6), 441–461.
- Schimmelpennig, I., Benedetti, L., Garreta, V., Pik, R., Blard, P.-H., Burnard, P., Bourlès, D., Finkel, R., Ammon, K., Dunai, T., 2011. Calibration of cosmogenic <sup>36</sup>Cl production rates from Ca and K spallation in lava flows from Mt. Etna (38°N, Italy) and Payun Matru (36°S, Argentina). *Geochim. Cosmochim. Acta* 75 (10), 2611–2632.
- Schmid, S.M., Fügenschuh, B., Kounov, A., Maženco, L., Nievergelt, P., Oberhänsli, R., Pleuger, J., Schefer, S., Schuster, R., Tomljenović, B., Ustaszewski, K., van Hinsbergen, D.J.J., 2020. Tectonic units of the Alpine collision zone between Eastern Alps and western Turkey. *Gondwana Res.* 78, 308–374.
- Sebe, K., Csillag, G., Ruzsiczay-Rüdiger, Z., Fodor, L., Thamó-Bozsó, E., Müller, P., Braucher, R., 2011. Wind erosion under cold climate: A Pleistocene periglacial megarand system in Central Europe (Western Pannonian Basin, Hungary). *Geomorphology* 134 (3-4), 470–482.
- Sebe, K., Roetzel, R., Fiebig, M., Lütthgens, C., 2015. Pleistocene wind system in eastern Austria and its impact on landscape evolution. *Catena* 134, 59–74.
- Seltzer, A.M., Ng, J., Aeschbach, W., Kipfer, R., Kulongoski, J.T., Severinghaus, J.P., Stute, M., 2021. Widespread six degrees Celsius cooling on land during the Last Glacial Maximum. *Nature* 593 (7858), 228–232.
- Sissons, J.B., 1974. A late-glacial ice-cap in the central Grampians. Scotland. *Trans. Inst. Br. Geogr.* 62, 95–114.
- Shakun, J.D., Carlson, A.E., 2010. A global perspective on Last Glacial Maximum to Holocene climate change. *Quat. Sci. Rev.* 29 (15-16), 1801–1816.
- Smith, G.W., Nance, R.D., Genes, A.N., 1997. Quaternary glacial history of Mount Olympus. Greece. *Geol. Soc. Am. Bull.* 109, 809–824.
- Smith, G.W., Nance, R.D., Genes, A.N., 2006. Pleistocene glacial history of Mount Olympus, Greece: Neotectonic uplift, equilibrium line elevations, and implications for climatic change. *Geol. Soc. Am. Spec. Pap.* 409, 157–174.
- Spratt, R.M., Lisiecki, L.E., 2016. A Late Pleistocene sea level stack. *Climate of the Past* 12, 1079–1092.
- Steier, P., Martschini, M., Buchriegler, J., Feige, J., Lachner, J., Merchel, S., Michlmayr, L., Priller, A., Rugel, G., Schmidt, E., Wallner, A., 2019. Comparison of methods for the detection of <sup>10</sup>Be with AMS and a new approach based on a silicon nitride foil stack. *Int. J. Mass Spectrom.* 444, 116175.
- Stone, J.O., 2000. Air pressure and cosmogenic isotope production. *J. Geophys. Res.* 105 (B10), 23753–23759.
- Sümeği, P., Gulyás, S., 2021. Some notes on the interpretation and reliability of malacological proxies in paleotemperature reconstructions from loess - comments to Obrecht et al.'s "A critical reevaluation of paleoclimate proxy records from loess in the Carpathian Basin". *Earth Sci. Rev.* 221, 103675.
- Temovski, M., Pruner, P., Hercman, H., Bosák, P., 2016. Cave response to environmental changes in Late Pleistocene: study of Budimirica Cave sediments. Macedonia. *Geol. Croat.* 69, 307–316.
- Temovski, M., 2018. Ice caves in FYR of Macedonia. In: Persoiu, A., Lauritzen, S.E. (Eds.), *Ice Caves*. Elsevier, pp. 455–478.
- Temovski, M., Madarász, B., Kern, Z., Milevski, I., Ruzsiczay-Rüdiger, Z.s., 2018. Glacial Geomorphology and Preliminary Glacier Reconstruction in the Jablanica Mountain, Macedonia, Central Balkan Peninsula. *Geosci.* 8, 1–21.
- Thomas, F., Godard, V., Bellier, O., Shabanian, E., Ollivier, V., Benedetti, L., Rizza, M., Espurt, N., Guillou, V., Hollender, F., Molliex, S., 2017. Morphological controls on the dynamics of carbonate landscapes under a mediterranean climate. *Terra Nova* 29 (3), 173–182.
- Tierney, J.E., Zhu, J., King, J., Malevich, S.B., Hakim, G.J., Poulsen, C.J., 2020. Glacial cooling and climate sensitivity revisited. *Nature* 584 (7822), 569–573.
- Varsányi, I., Palcsu, L., Kovács, L.Ó., 2011. Groundwater flow system as an archive of palaeotemperature: Noble gas, radiocarbon, stable isotope and geochemical study in the Pannonian Basin. Hungary. *Applied Geochem.* 26 (1), 91–104.
- Vieira, G., 2008. Combined numerical and geomorphological reconstruction of the Serra da Estrela plateau icefield, Portugal. *Geomorphology* 97 (1-2), 190–207.
- Vojnogeografski institut, 1973. Topographic maps in 1:25000 scale, sheets: Skopje 1-1 to Skopje 4-4 sheets, SFR Yugoslavia, Belgrade.
- Weertman, J., 1971. Shear stress at the base of a rigidly rotating cirque glacier. *J. Glaciol.* 10 (58), 31–37.
- Zasadni, J., Klapya, P., 2014. The Tatra Mountains during the last glacial maximum. *J. Maps* 10 (3), 440–456.
- Zasadni, J., Klapya, P., Świąder, A., 2018. Predominant western moisture transport to the Tatra Mountains during the last glacial maximum, inferred from glacier palaeo-ELAs. XXI International Congress of the CBGA, Salzburg, Austria.
- Zasadni, J., Klapya, P., Broš, E., Ivy-Ochs, S., Świąder, A., Christl, M., Balázovičová, L., 2020. Latest Pleistocene glacier advances and post-Younger Dryas rock glacier stabilization in the Mt. Kriván group, High Tatra Mountains, Slovakia. *Geomorphology* 358, 107093.
- Zasadni, J., Klapya, P., Kaluza, P., Świąder, A., 2021. Evolution of the Białka valley Pleistocene moraine complex in the High Tatra Mountains. *Catena* 207 (105704), 1–19.
- Žebre, M., Stepišnik, U., 2014. Reconstruction of Late Pleistocene glaciers on Mount Lovćen. Montenegro. *Quat. Int.* 353, 225–235.
- Žebre, M., Sarikaya, M.A., Stepišnik, U., Yıldırım, C., Çiner, A., 2019. First <sup>36</sup>Cl cosmogenic moraine geochronology of the Dinaric mountain karst: Velež and Crvanj Mountains of Bosnia and Herzegovina. *Quat. Sci. Rev.* 208, 54–75.
- Žebre, M., Sarikaya, M.A., Stepišnik, U., Colucci, R.R., Yıldırım, C., Çiner, A., Candaş, A., Vlahović, I., Tomljenović, B., Matoš, B., Wilken, K.M., 2021. An early glacial maximum during the last glacial cycle on the northern Velebit Mt. (Croatia). *Geomorphology* 392, 107918.
- Zerathe, S., Braucher, R., Lebourg, T., Bourlès, D., Manetti, M., Léanni, L., 2013. Dating chert (diagenetic silica) using in-situ produced <sup>10</sup>Be: Possible complications revealed through a comparison with <sup>36</sup>Cl applied to coexisting limestone. *Quat. Geochronol.* 17, 81–93.
- Zickel, M., Becker, D., Verheul, J., Yener, Y., Willmes, C., 2016. Paleocoastlines GIS dataset; computed land masks of past sea level models. CRC806-Database, 10.5880/SFB806.20.